SPECTRAL ANALYSIS OF PETROLEUM RESERVOIR ROCK USING FOURIER TRANSFORM INFRARED (FTIR) SPECTROSCOPY

By

LOGAN CHATTERTON

Bachelor of Science Geology

Oklahoma State University 2013

Stillwater, OK

2013

Submitted to the Faculty of the
Graduate College of the
Oklahoma State University
in partial fulfillment of
the requirements for
the Degree of
MASTER OF SCIENCE
July, 2015

HYPERSPECTRAL ANALYSIS OF PETROLEUM RESERVOIR ROCK USING FOURIER TRANSFORM INFRARED (FTIR) SPECTROSCOPY

Thesis Approved:

Dr. Jeffrey M. Byrnes

Thesis Adviser

Dr. Mohamed Abdelsalam

Dr. Jack Pashin

ACKNOWLEDGEMENTS

I would first and foremost like to thank my advisor for the past four years through my undergraduate and graduate career here at the Oklahoma State University Boone Pickens School of Geology, Dr. Jeffrey Byrnes. This project began as an undergraduate research project and cultivated into an encompassing thesis that has been both rewarding and challenging, and he has been there every step of the way. I would like to say thank you to Steve Chipera at Chesapeake Energy for providing a core and XRD data for this study as well as being there to help me with questions when I ran into speed bumps. I would also like to thank Hannah Hill who helped out with my work this past semester. I would like to thank the Boone Pickens School of Geology, the Erik Mason Fellowship Committee, and Mr. and Mrs. Rick Ely for graciously funding me and allowing me to study here at OSU. I would like to thank all of my friends here at OSU, the past two years have been life changing, and it would not have been the same without everyone. I would like to sincerely thank Dr. Jim Puckette. Six years ago I started my college career with a plan that would not have led me to where I am today. I fell in love with geology after taking one introductory course taught by Dr. Puckette and have never looked back. He has always been around sparking my curiosity and there to answer my questions. Last but not least, I need to thank my family for their continual support and helping to push me farther than I knew I could go. Finally, I would like to thank my committee members Dr. Jack Pashin, and Dr. Mohamed Abdelsalam for their advice along the way.

Name: Logan Chatterton

Date of Degree: JULY, 2015

Title of Study: HYPERSPECTRAL ANALYSIS OF PETROLEUM RESERVOIR ROCK USING FOURIER TRANSFORM INFRARED (FTIR) SPECTROSCOPY

Major Field: GEOLOGY

Abstract:

Compositional analysis of reservoir rock is a vital aspect of oil exploration and production activities. In a broad sense, knowing the mineral composition of a reservoir can help with characterization and interpretation of depositional environments. On a smaller scale, identifying mineralogy helps calibrate well logs, identify formations, design drilling and completion programs, and screen for intervals with potential problem minerals, such as swelling clays. The petroleum industry utilizes two main methods to find compositional mineralogy, x-ray diffraction (XRD) and thin section analysis. Both methods are time consuming, expensive, and destructive. An alternative method for compositional analysis that includes quantitative mineralogy is a valuable prospect, especially if it had the potential to characterize the total organic content (TOC).

The remote sensing community has been using infrared spectroscopy to analyze mineralogy for years. Within the last ten years, the advancement of infrared spectrometers and processing programs have allowed infrared spectra to be taken and analyzed faster and easier than before. The objective of this study is to apply techniques used in remote sensing for quantitatively finding mineralogy to the petroleum industry. While developing a new methodology to compositionally analyze reservoir rock, a database of infrared spectra of relevant minerals has been compiled. This database was used to unmix spectra using a constrained linear least-squares algorithm that is used in the remote sensing community. A core has been scanned using a hand-held infrared spectrometer. Results of the best method show RMS error from mineral abundance to be under five percent.

TABLE OF CONTENTS

Chapter Page

LIST OF TABLES

Table Page

LIST OF FIGURES

Figure Page

CHAPTER I

INTRODUCTION

a. Project Motivation

Compositional analysis of reservoir rock is a vital aspect of petroleum exploration and production. In a broad sense, knowing the mineral composition of a reservoir can help with characterization and interpretation of facies, depositional processes, and paleoenvironments. On a smaller scale, identifying mineralogy aids to calibrate logs, pick formations, design drilling and completion strategies, and screen for intervals with problem minerals, such as swelling clays (Adam et al., 1988). The petroleum industry uses two main methods to determine the mineralogy of reservoir rocks: thin section analysis and X-ray diffraction (XRD). Both methods are time consuming, expensive, and destructive. Thin section analysis relies on sample preparation and is an operator-dependent technique that uses point counting to determine bulk mineralogy. This technique typically requires at least days to weeks for sample preparation and analysis (Adam et al., 1988). XRD also can take days for sample preparation and analysis. Mud loggers can give an on-site real time perspective on mineralogy and lithology using drill cuttings as a well is drilled. However, the quality of this method is operator-dependent, making results highly variable.

As drilling technology and recovery techniques continue to advance, the turnaround time for compositional analysis of samples is increasingly of the uttermost importance. An alternate method for analyzing mineralogy that is time efficient, inexpensive, nondestructive, and not

operator-dependent would be extremely valuable. In order to make such an alternative feasible, this investigation focuses on developing a technique to compositionally analyze reservoir rock for the petroleum industry using infrared (IR) spectroscopy.

Shale can be characterized by texture, grain size, or composition. For this study, *shale* is defined as an indurated, fissile, fine-grained mudrock with the majority of the grains being silt sized (less than 62.5 microns) (Picard, 1971; Lewan, 1978; Lundegard and Samuels, 1980). Other classification schemes look at the mineralogy of the shale for classification. Specific minerals within shale are known for variable mechanical and chemical stability (Loucks et al., 2012). Carbonates, feldspars, and phosphates are mechanically stable but chemically unstable and can be dissolved by formation fluids during diagenesis. Clay minerals are considered mechanically and chemically unstable due to swellability, compactibility, and pliability, as well as potential mobility within a porous rock matrix. Mechanically and chemically stable minerals in the subsurface include silica and pyrite. However, each of these materials affect production differently. Production geologists and engineers seek rocks brittle enough to fracture hydraulically and stay propped open following stimulation. Mineralogy is one of the main factors for determining if a rock will fracture and maintain high secondary permeability during production.

b. Purpose and Objectives

Thermal infrared (TIR) spectroscopy provides an effective, nondestructive way to analyze the surface of geologic materials (e.g., Byrnes et al., 2007). The first attempt to find rock composition from crushed or powdered samples was done in the 1950's by *Hunt and Turner* (1953) and *Lyon* (1959). As the science of geochemical analysis using spectrometers progressed, the fundamentals were incorporated more broadly into remote sensing. In the last ten years, advancements in spectrometer technology and software have opened this remote sensing field

from a few experts to a wider portion of the remote sensing community (Kruse, 1996). The purpose of this study is to apply previously tested remote sensing methods of finding mineralogy to oilfield reservoir rocks. My methods will be applied to the Dulcey BRA 5H core from the Devonian-age Marcellus Shale of Bradford County, Pennsylvania, which was supplied by Chesapeake Energy.

My main research objectives are as follows:

1. Compare spectra generated by the Exoscan Fourier Transform Infrared (FTIR) spectrometer to other spectral libraries such as the Arizona State University (ASU) Thermal Emission Spectroscopy (TES) Laboratory Spectral Library, the United States Geological Survey's (USGS) Digital Spectral Library, and the John Hopkins University Spectral Library.
2. Optimize a spectral endmember library that allows for quantitative compositional analysis.
3. Develop a method to interpret the spectral significance of total organic carbon (TOC).
4. Determine the best method to unmix (i.e., spectrally deconvolve) spectra.
5. Develop a technique to compositionally analyze reservoir rock by synthesizing FTIR spectroscopy with XRD data.

c. Application

As previously stated, my methods will be applied to the Dulcey BRA 5H (Figure 1). The core contains a series of clay-rich (illite, illite/smectite mixed layer, and chlorite), quartz-rich, and carbonate-rich zones. Identification of these zones is an essential part of reservoir characterization and is useful for identifying completion zones and developing production strategies. Further identification of the specific feldspars could also yield important information to help determine

depositional environment. The Marcellus Formation was deposited in the Appalachian Basin during the Middle Devonian. The Marcellus Formation encompasses parts of two transgressive-regressive cycles (Lash and Engelder, 2011). The Appalachian Basin is categorized as a foreland basin, which subsided as a result of the Acadian Orogeny loading the Laurentian craton (Brett and Baird, 1996). The first box of the core is shown in Figure 2.

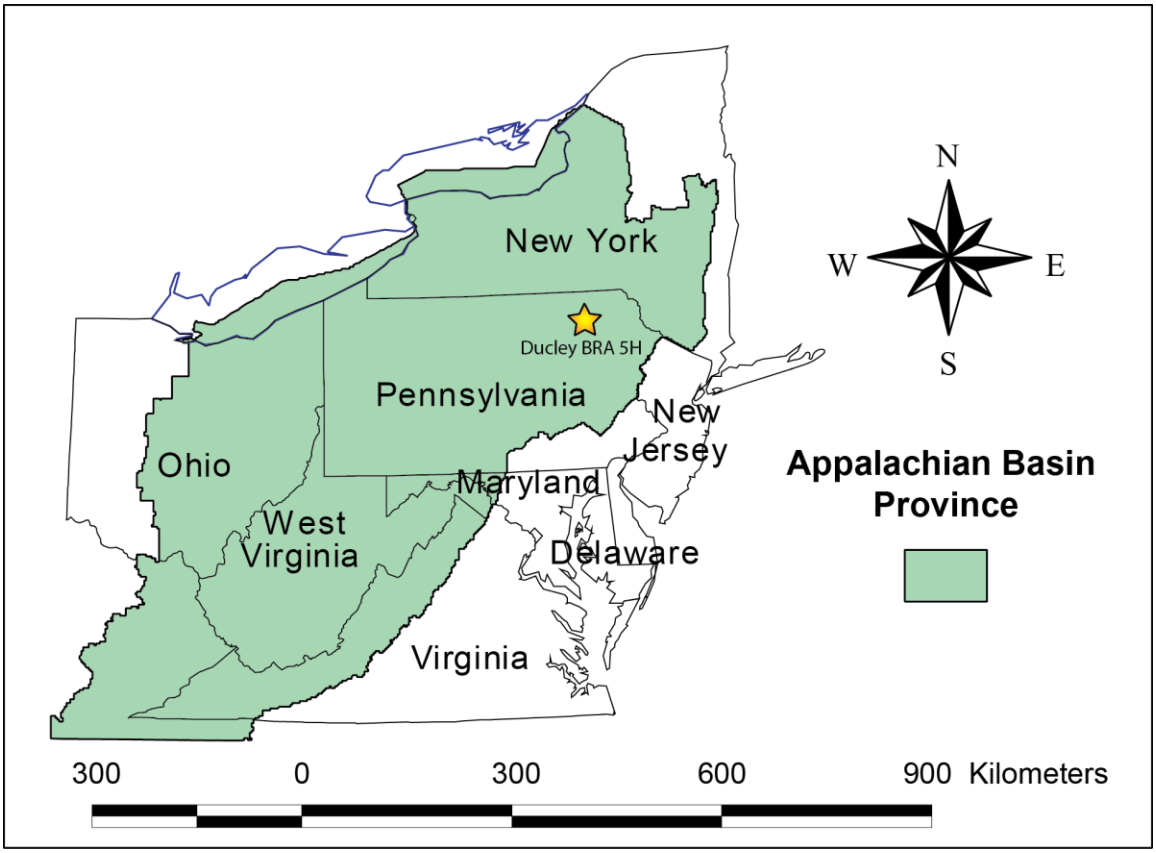

Figure 1: Approximate Dulcey BRA 5H core location, Bradford County, Pennsylvania (modified from Milici and Swezey (2006)).

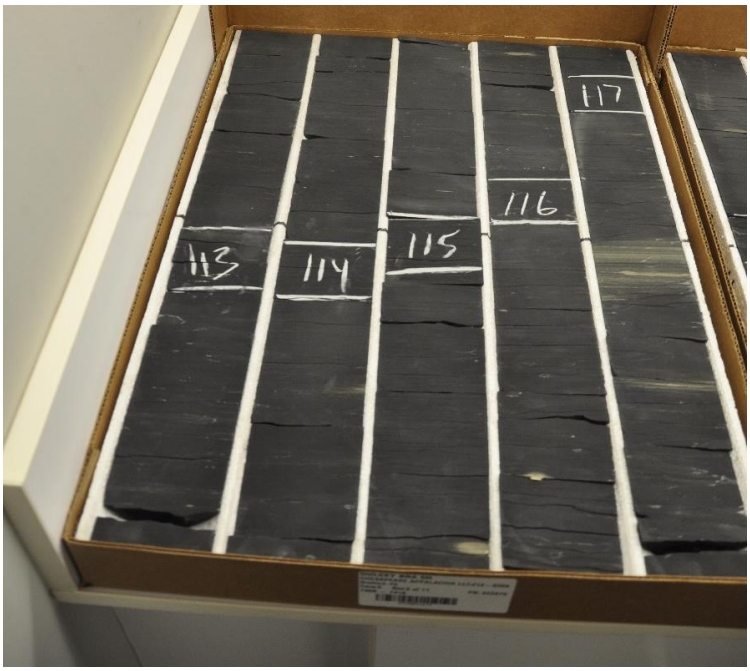

Figure 2: Dulcey BRA 5H core. Chalked intervals were used for XRD analysis.

CHAPTER II

BACKGROUND

a. Infrared (IR) Spectroscopy

The wavelength region used in this study, and common in many others, is the mid-infrared portion of the IR region, which occurs within 4000-400 cm^{-1} (2.5-25 μm) (Matteson and Herron, 1993). When electromagnetic radiation interacts with a mineral, the energy is either reflected, absorbed, or transmitted. When the energy is absorbed by geologic material, it is converted to vibrational energy (Adam et al., 1988); the energy is then radiated by the material because it cannot heat up indefinitely. Vibrational motion is measured at specific frequencies that are directly related to the crystal structure and composition of the material (i.e., mineralogy) (Christensen et al., 2000). Figure 3 shows an IR spectrum of illite. The vibrational motions produce the observed spectral features (i.e., peaks and troughs in the spectrum). These spectral features are caused by energy loss at characteristic vibrational modes (Sondergeld and Rai, 1993). Because each mineral has its own characteristic spectrum, a rock will be a combination, or mixture, of mineral spectra (plus any other material components in the rock). Mineralogy can then be determined using an unmixing technique. The combined sets of peaks and troughs in a spectrum are diagnostic of qualitative bulk mineralogy (Lyon, 1963). The depths of the peaks and troughs are indicative of the quantitative modal composition of the rock (Lyon and Burns, 1963). Based on the theoretical and empirical evidence that an IR spectrum of a geologic material (such

as a rock) is a weighted linear combination of the spectra of its components (Feely and Christensen, 1999), it is possible to use a linear regression to find mineral composition.

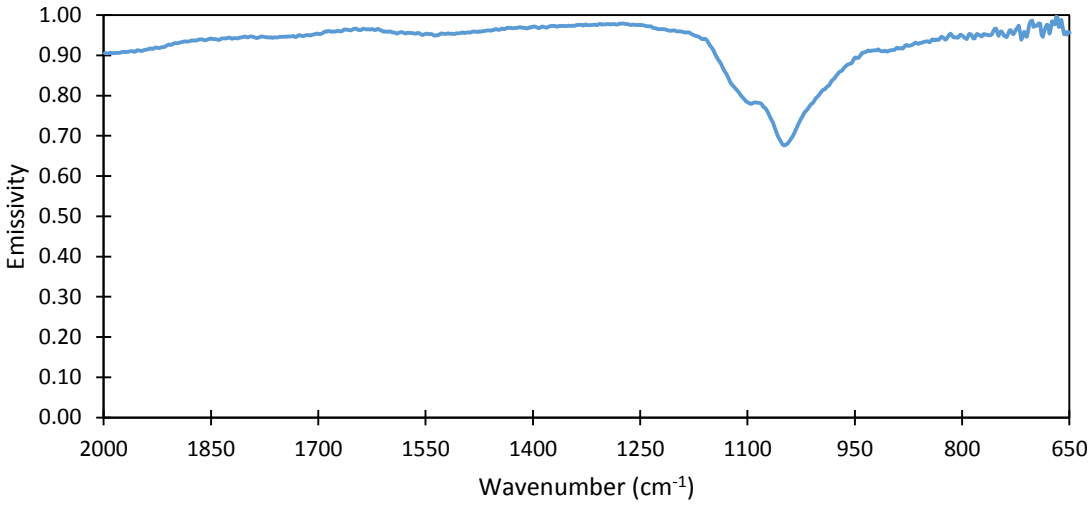

Figure 3: FTIR spectrum of illite.

b. Emission, Reflectance, and Absorption

Several vibrational IR spectroscopy techniques have been demonstrated to yield quantitative mineralogy results using transmission, reflectance, absorbance, emission, and Raman methods. Previous studies related to the petroleum industry have successfully used IR absorbance to quantitatively determine a sample's mineralogy (Adam et al., 1988; Matteson and Herron, 1993; Sondergeld and Rai, 1993; Ballard, 2007; Adamu, 2010). Other studies in remote sensing have used or compared IR emissivity and reflectance of geologic materials (Ramsey and Christensen, 1998; Christensen et al., 2000; Byrnes et al., 2007; Byrnes and Byrnes, 2011); these studies have also demonstrated that unmixing techniques are accurate for compositional mineral analysis.

A blackbody is a theoretical material that absorbs 100% of thermal energy radiated onto it, does not reflect any energy, and emits thermal energy with 100% efficiency (Hapke, 1993).

This shows that reflectance and emission are inversely related. Because the geologic materials under study are opaque there is no thermal radiation transmitted, thus the fraction of reflected energy plus the fraction of absorbed energy equals one (Incropera et al., 2011). Kirchhoff's Law states emissivity is equal to one minus reflectance (Salisbury et al., 1994). Using this principle, spectra found by measuring reflectance can be converted to emissivity.

c. Unmixing Method

As previously stated, spectra of rocks can be viewed as a weighted linear combination of infrared component spectra. This principle allows two important conclusions. First, a rock with known mineral composition can be modeled by a weighted linear mixing of spectra. Second, a linear deconvolution, or unmixing, can provide mineral abundances for a sample with unknown minerals composition (Hunt and Turner, 1953; Ramsey, 1996; Ramsey and Christensen, 1998; Feely and Christensen, 1999). The unmixing algorithm used herein has previously been applied to emissivity spectra of mineral mixtures of various numbers and particle sizes to test the limits of linear deconvolution of thermal emission spectra (e.g., Ramsey and Christensen, 1998). The deconvolution is achieved by using least squares (LS) regression analysis to solve a system of equations created from the rock and mineral emissivity spectra (Ramsey and Christensen, 1998).

d. Previous Techniques

Multiple regression analysis techniques have been developed to unmix a sample's spectrum into mineral percentages. Matteson and Herron and others (Matteson and Herron, 1993; Herron et al., 1997; Herron et al., 1998) use a least squares (LS) and non-negative least squares (NNLS) regression to solve for mineralogy in MATLAB. This technique was applied to transmission spectra acquired by scanning KBr pellets. These pellets are made by crushing wanted minerals to a desired particle size. The minerals are then added to KBr powder and pelletized. The least squares regression is unconstrained and can have negative products. Non-

negative least squares regression is constrained only in the fact that it will not produce negative numbers abundances. They found that the average absolute error using least squares was ± 2.6 wt. %, and non-negative least squares the average absolute error was ± 1.2 wt. % (Matteson and Herron, 1993).

Ramsey (1996) used a constrained least squared linear retrieval algorithm that allows for a modeled best fit spectral endmember percentage of a given mixture. The algorithm used is shown by Equation 1.

$$\varepsilon(\lambda)_{mixture} = \sum_{i=1}^{n} \zeta_i \varepsilon(\lambda)_i + \delta(\lambda) \qquad \text{Equation 1.}$$

The created model is shown by $\varepsilon(\lambda)_{mixture}$, the areal fraction of each endmember is shown by $\zeta_i \varepsilon(\lambda)_i$, and then the residual error is $\delta(\lambda)$. Each endmember fraction when summed must equal unity, displayed by the created model. The residual error is calculated at each wavenumber and usually converted to root mean square (RMS) error. Equation 1 shows that equations are run at each wavenumber for each endmember. Endmembers that result in negative values using this method are thrown out and the deconvolution is then rerun. This method does not allow for a solution without the endmembers totaling unity. Other methods run a renormalization of the endmember fractions as the last step in the unmixing process (Johnson et al., 1992).

Kruse also uses employs a constrained and unconstrained LS algorithm (Kruse et al., 1993; Kruse, 1996). Kruse uses this method on split core to find mineralogy. He took more of an image analysis approach and created a hyperspectral image by making a grid of a core face. Each scan in the grid is seen as a pixel within a spectral image. Then, the synthetic image is unmixed. This allows for easier visualization of mineral distribution over the scanned core.

CHAPTER III

METHODOLOGY

A method of hyperspectral unmixing was adapted to compositionally analyze reservoir rock. It utilizes FTIR spectroscopy to quantitatively find mineralogy as well an attempt to interpret the spectral significance of total organic carbon (TOC). This method was tested by comparing modeled mineral percentages (produced by spectral unmixing) to XRD data supplied by Chesapeake Energy.

a. Measuring Core

FTIR spectra of the Dulcey BRA 5H core were obtained using a 4100 ExoScan FTIR spectrometer (Agilent Technologies). The Exoscan uses an active source within the spectrometer to radiate infrared energy on a sample. The reflected energy is then measured (approximately hemispheric) and divided by reflectance from a diffuse gold standard to produce an FTIR spectrum. The core was measured at intervals corresponding roughly to where XRD samples were collected. Figure 4 shows zones that were chalked off as XRD samples. Spectra were initially planned to be collected by placing the FTIR spectrometer on the core face, as demonstrated in Figure 5. In this sampling geometry, the diffuse component of reflectance was not sufficient because of the smooth face of the cut core. Instead, broken pieces of the core within the corresponding XRD sample zones were taken and placed on the spectrometer to measure a diffuse reflection. Figure 6 shows the stand used while measuring core pieces. The pieces were

measured perpendicular to bedding. The pieces are likely broken due to bedding failures during or after the core was retrieved from the subsurface. This is caused by the preferential arrangement of clay particles along bedding planes (Ingram, 1953). The ExoScan FTIR is supplied with Agilent MicroLab Mobile software, which allows the instrument to run calibrations and system tests, record spectra, and export data. Each time the Exoscan is turned on, a crystal test is run and a background scan is collected. The background scan is used to correct atmospheric variances associated with water vapor or carbon dioxide. The FTIR spectrometer is set to run for 256 scans (for both background and sample collections) at the maximum spectral resolution of 4 cm^{-1}. The spectral range collected was from 4000 - 650 cm^{-1}.

Figure 4: Third box of core from Dulcey BRA 5H; depth ranges from 7428-7438 ft.

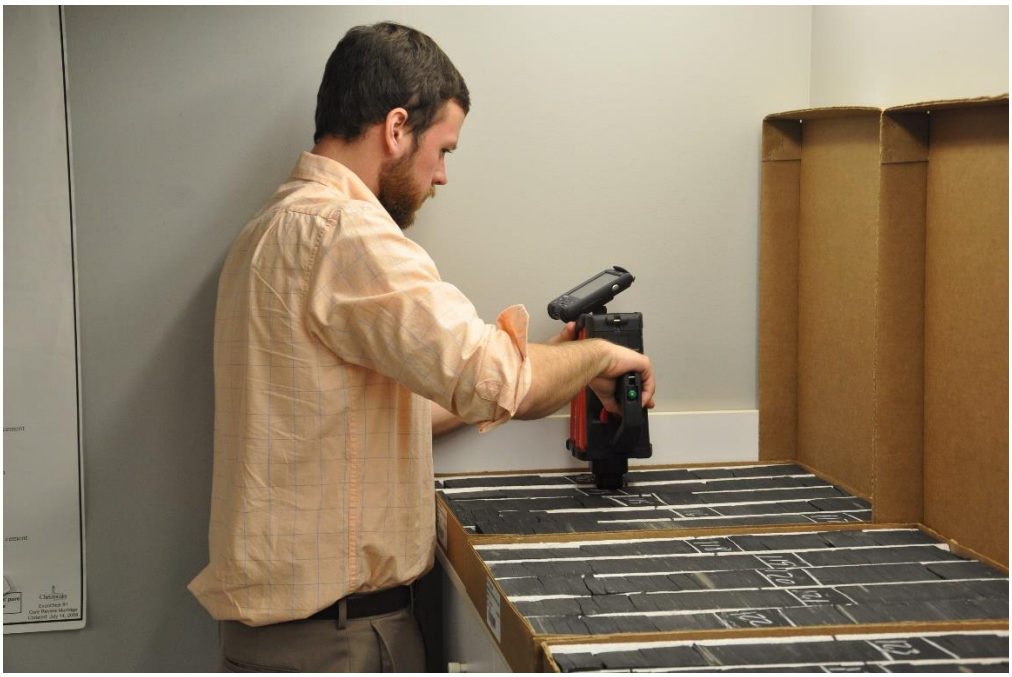

Figure 5: Measuring the core using the 4100 FTIR ExoScan.

Figure 6: ExoScan stand with a core piece being measured perpendicular to bedding.

b. Unmixing Packages

Use of three different spectral unmixing packages was attempted for spectral deconvolution in this study. Spectral mixture analysis (SMA) is a technique used in remote sensing that analyzes each pixel of an image in an attempt to derive the fractional percentages of the components (minerals, vegetation, water, and atmospheric variances) in an image (Wessman et al., 1997). However, problems arose while inputting the first SMA package. Packages used for spectral unmixing are normally used for images, not for deconvolution of a single mixed spectrum. The first SMA was only able to unmix images and was therefore not applicable for this study. The next package that was tested was VIPER tools. VIPER tools is an open-source spectral mixture analysis software. It uses a technique known as multiple endmember spectral mixture analysis (MESMA). This technique was developed and tested by Roberts et al. (1998) for analysis of the Santa Monica Mountains using Airborne Visible/Infrared Imaging Spectrometer (AVIRIS) data. VIPER tools is written to be used in the Environment for Visualizing Images (ENVI) software package. The package was downloaded as an interactive data language (IDL) script and was then incorporated as a subscript in ENVI. The first attempts at unmixing using VIPER tools produced no results. Like SMA, MESMA is normally used for spectral image analysis instead of analyzing a single spectrum. The third package, previously described, is called jENVI. The unmixing algorithm was initially written in FORTRAN for fast computational analysis (Ramsey and Christensen, 1998) and was then rewritten in IDL (Piatek and Moersch, 2006) for use with ENVI. jENVI has three different unmixing modes: (1) single spectrum analysis, (2) simultaneous analysis of multiple spectra using the same endmember library, and (3) analysis of an entire image. The bands in the mixed spectrum must be spectrally equivalent (in wavelength region, spectral resolution, etc.) to the bands in the endmember library for deconvolution. Endmembers can be selected or deselected as components before and after each unmixing. The use of a blackbody as a component is also an option. Unmixing iterations were run based on a constrained

model. This means the algorithm ignores any endmember that are negative. jENVI also allows the user to choose what percentage to use for a cutoff. I allowed the models to return all values of components used.

c. Endmember Library Creation

An endmember library was created based on the minerals found by the XRD results, .including quartz, potassium feldspars, plagioclase feldspars, apatite, pyrite, calcite, dolomite, illite-smectite mixed layer, illite/mica, and chlorite. XRD is unable to distinguish specific minerals within the potassium feldspar and plagioclase feldspar groups. Illite and mica also have the same spectral feature and are grouped together. The XRD results also include a TOC component percentage.

Using the minerals provided via XRD analysis as a starting point, several online infrared spectral libraries were included in order to produce accurate spectral models. The Arizona State University (ASU) Thermal Emission Spectroscopy (TES) Laboratory Spectral Library is an online spectral library that exports in digital form. Descriptions of samples include degree of purity, visual identification, bulk oxides, microprobe oxides, XRD analysis, and particle size (Christensen et al., 2000). The spectra were collected with a Matteson Cygnus 100 interferometric spectrometer that was adapted from transmission to emission capabilities (Christensen et al., 2000). Spectra exported from this library are exported with a spectral range of 2000-200 cm^{-1}, with 923 bands. These files were then resampled to match the spectral range and resolution of 2000 - 650 cm^{-1} with 723 bands.

The John Hopkins University (JHU) Spectral Library contains spectra of materials including terrestrial rocks, minerals, lunar soils, terrestrial soils, manmade materials, meteorites, and vegetation. The minerals in the library were measured in bidirectional reflectance (Salisbury and Vergo, 1991). The mineral library spectral range is 4807.7-399.4 cm^{-1} with 2287 bands

(Baldridge et al., 2009). The John Hopkins spectral library is included with ENVI. Because the spectra in this study were measured in reflectance, Kirchhoff's Law (E=1-R) was used to convert the spectra to emissivity (Nicodemus, 1965).

Finally, the United States Geological Survey's (USGS) digital spectral library was also used, which includes spectra collected using a Nicolet FTIR spectrometer (Clark et al., 2007). This instrument measures in biconical reflectance. The spectral range is 7806.48 - 46.27 cm^{-1} (1.28 – 216 μm) with 4025 bands. Since the spectra from the USGS spectral library were collected using reflectance, they were also converted to emissivity spectra using Kirchhoff's Law.

Spectra were also collected in the Oklahoma State University (OSU) Remote Sensing Laboratory (4000-650 cm^{-1} with 1795 bands) using the same FTIR spectrometer used to measure the core from Chesapeake Energy. Mineral hand samples were placed on the stand, and spectra were collected using the same method for sampling the core. Previously created pressed mineral sample pellets were also measured and input to the endmember library to test for sample variability. Finally, emissivity spectra from all sources were resampled to 2000-650 cm^{-1} with 723 bands.

d. Data Conversion

Chesapeake provided XRD data (expressed as mineral weight percents) for the odd core samples that were measured (14 measurements). Because the FTIR measurements are in volume percent, a conversion was needed to use the XRD data. This was done by dividing the original weight percentage by the mineral's specific gravity (Klein et al., 2002). That number was then divided by the sum of the original weight percent divided by the specific gravity of each mineral. Table 1 shows an example of the conversion for sample 113. This was done for every sample individually. Because of the wide range in densities of organic materials represented within TOC, a ratio equation was used to solve for densities for each sample. Each sample then used a specific

TOC density for further conversion; TOC specific gravity ranged from 2.71 to 2.91 and averaged 2.81.

Table 1: Conversion of weight percent to volume percent for each of the 11 components present in sample 113.

Sample ID 113
Sample Depth 7409.16

Sample	wt. %	specific gravity	$cm^3/100g$	total volume/100g	vol. %
Quartz	29.7	2.65	11.207547	36.250081	30.917302
K-Feldspar	0.4	2.57	0.155642	36.250081	0.4293563
Plagioclase	9.3	2.71	3.4317343	36.250081	9.4668322
TOC	4.1	2.82	1.4539007	36.250081	4.0107516
Apatite	0.3	3.00	0.1	36.250081	0.2758615
Pyrite	4.7	5.02	0.936255	36.250081	2.5827666
Calcite	1.8	2.71	0.6642066	36.250081	1.8322901
Dolomite	2.9	2.85	1.0175439	36.250081	2.8070113
Mixed Layer	6.0	2.90	2.0689655	36.250081	5.7074783
Illite + Mica	40.0	2.69	14.880952	36.250081	41.050811
Chlorite	1.0	3.00	0.3333333	36.250081	0.9195382

e. Forward Mixing

Using the created endmember library, forward mixture models were synthesized using weighted averages of each mineral component spectrum based on the volumetric abundances converted from the XRD data provided by Chesapeake Energy. Each forward mixing model was then visually compared to the measured spectrum from the core by plotting them together. Each model was also statistically compared by finding the absolute difference between modeled and measured spectra as computed by the root mean square (RMS) error. Conditional formatting was also used for visual aid of variance between the modeled and measured spectra. As previously stated, the accuracy of the forward mixing depends on having the correct spectra in the endmember library. To get more accurate models, different mineral spectra were tested in the weighted averaging. Comparisons for each different mineral spectra were done visually and

statistically. Multiple different spectra were tested for each measured core sample. The lower the RMS, the more accurate that mineral's spectrum was for the mixing, and theoretically, a better representative spectra for later unmixing. These statistical comparisons were done for multiple mineral spectra in the endmember library for every XRD sample provided. The 10 mineral spectra used in the forward mixing modeling are termed as the RMS Forward-Mixed Library for unmixing. To represent the overall Marcellus Shale core, all 25 FTIR spectra of the core were averaged. Using the method described above, a separate forward mixing library was then created called the Averaged Shale Library, which was then used to model the measured core spectra by forward mixing.

f. Spectral Unmixing/Deconvolutions

Unmixing was done using jENVI for single spectrum analysis as previously described. To run the algorithm, a measured FTIR spectrum (of the core) is chosen for input to the model, as well as the endmember library to be used for unmixing. The model compares each band of the mixed spectrum to the corresponding bands of each endmember to produce a best fit model. A constrained, non-negative model, which included a blackbody as a component, and showed all percentages of endmembers used was run for each measured spectrum. This was included in the unmixing to help model measured components with decreased spectral contrast, which is typically a result of particle size effects. The products of each unmixing model include the measured spectrum, the modeled (unmixed) spectrum, and the variance between the two plotted next to each other. A table is also produced for each unmixed spectrum that shows the name and percentages of each endmember used, the normalized values, the blackbody weight, the root mean square (RMS) error and the endmembers not utilized. The table was then adapted to match the XRD results table. A chart was also made based on the results produced for easier visualization.

The method described above was used for four different unmixing techniques, each using or creating a different endmember library. Two of the techniques use pre-existing endmember libraries for unmixing, the other two techniques create endmember libraries through multiple deconvolution iterations. The deconvolutions using pre-existing spectral libraries are the forward mixing libraries (RMS Forward-Mixed Library, and the Averaged Shale Library) and a technique called blind unmixing. The blind unmixing technique was tested by utilizing every spectrum in the endmember library. The techniques that create endmember libraries through iterations are the hand-picked technique and modification techniques. The hand-picked unmixing was done by starting with the entire endmember library, but in between each iteration stopping and looking at all of the results and throwing out mineral spectra that could, or should not be used in unmixing based on the percentage of the endmember used, or by looking at the interval of the core for which the endmember is used. For example, if a high percentage of a certain quartz spectrum is used for a portion of the core that is more clay rich, that spectrum is thrown out and the deconvolution is re-run. This technique was iterated until results closely matched XRD results. The first modification technique started with the RMS Forward-Mixed Library and switched one mineral spectrum for another spectrum of the same mineral. Unmixing was then run and mineral abundances were noted. This was done for each of the ten mineral components until results were satisfactory. This library is called the modified forward mixed endmember library. A separate modification technique was used to account for mineral variability throughout the core. This was done by starting with the modified Forward-Mixed Library and adding complementary mineral spectra to the library. This library is called the modified hand-picked library. The modified hand-picked library was created as a result of the high interplay between spectra while deconvolving. The above methods were used on all sample measurements (113-135 and 157-158).

CHAPTER IV

RESULTS

a. Measuring Core

Spectra were collected for the Dulcey BRA 5H core from Chesapeake Energy at 26 samples (113-135 and 157-159). 14 of these samples have corresponding XRD results. Figures 7-9 show spectra for samples 121, 135b, and 159b, which are clay-rich, quartz-rich, and carbonate-rich respectively. Multiple spectra were gathered at samples 116, 118, 120, 122, 133, 135, 157, 158, and 159 due to poor spectra collection on either the first or second measurement. If multiple spectra were collected from a single sample, the subsequent spectra were distinguished as a, b, or c. The early spectra were confirmed to be inaccurate by comparing the results of the forward mixed models as well as the unmixed component abundances and were subsequently not considered.

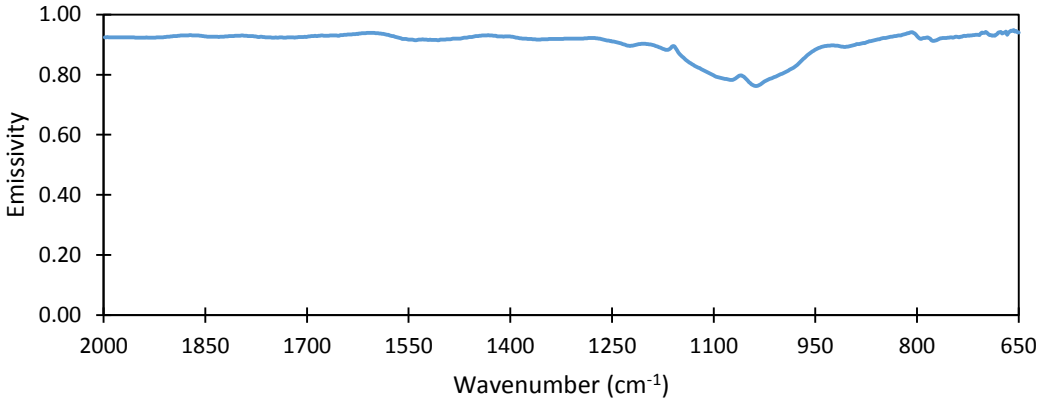

Figure 7: Spectrum collected for sample 121 (clay-rich).

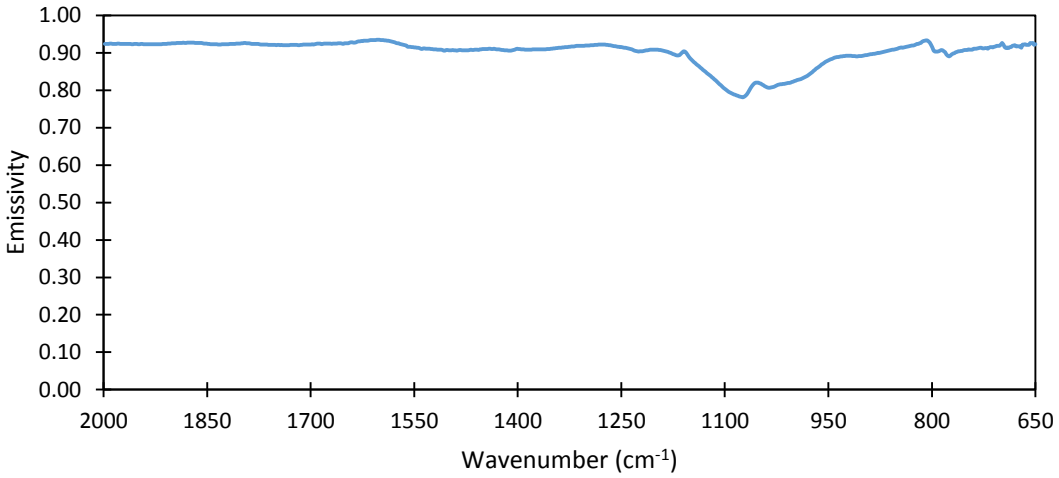

Figure 8: Spectrum collected for sample 135b (quartz-rich).

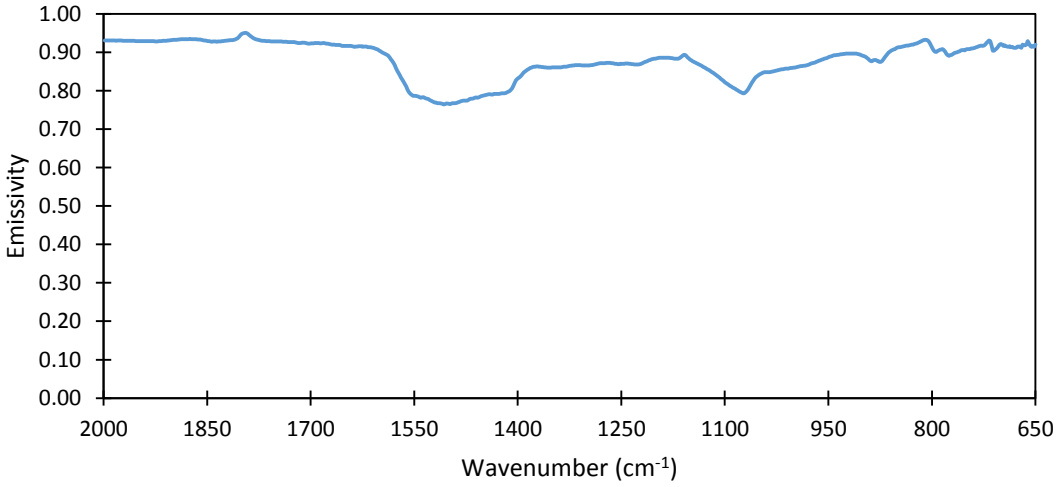

Figure 9: Spectrum collected for sample 159b (carbonate-rich).

b. Endmember Library Compilation

Using the minerals in the XRD table as a starting point, spectra were compiled and converted to a spectral library for future use. Secondary minerals were input to the library that were related to the minerals in the XRD table or reported to be in the Marcellus Formation (Potter et al., 1980). This process was repeated for all online infrared spectra sources. A spectral library

of 118 components was created for deconvolution. Figures 10-16 show plots of all the minerals or mineral groups that comprise the master endmember library (carbonates, quartz, K-feldspars, plagioclase feldspars, phyllosilicates, sulfides, phosphates). A full list of all minerals incorporated in the master endmember library is located in Appendix A. The main spectral feature that is diagnostic for carbonate minerals can be seen in Figure 10 at ~1600-1350 cm^{-1} with a secondary feature at ~900-850 cm^{-1}. The diagnostic spectral feature for quartz is at ~1300-1050 cm^{-1} with a secondary feature at ~810-770 cm^{-1} (Figure 11). Spectral features for K-feldspars are different for each mineral, but are typically ~1250-950 cm^{-1} (Figure 12). Plagioclase spectral features are also different for each specific mineral, but predominantly displayed at ~1250-900 cm^{-1} (Figure 13). Phyllosilicates display a dominant spectral feature at ~1250-930 cm^{-1}, but may also show lower emissivity at higher wavenumbers (Figure 14). Sulfides don't have any major spectral features, and are characterized by their near horizontal spectra (Figure 15). Phosphates have spectral features similar to the doublet displayed in quartz spectra, but it is shifted to lower wavenumbers (1175-975 cm^{-1}; Figure 16).

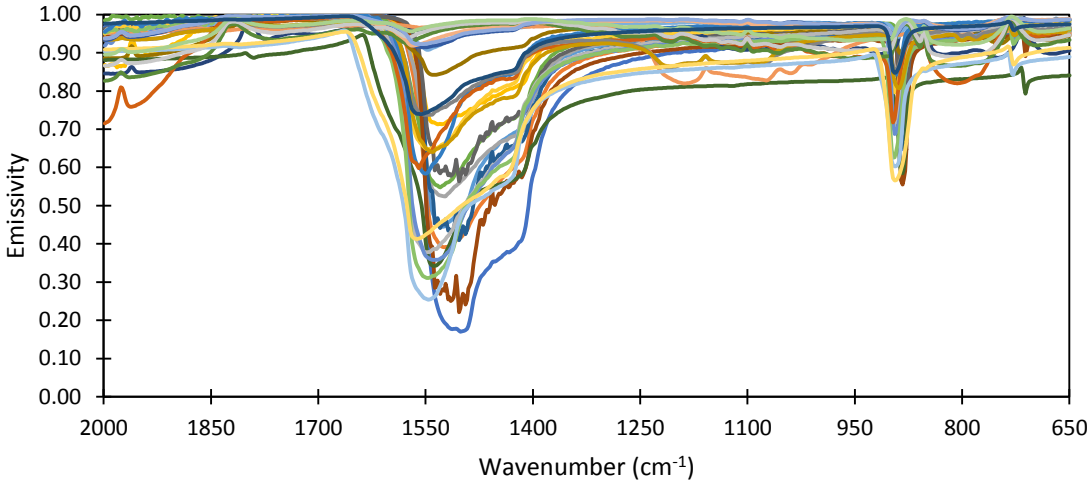

Figure 10: Plot of all carbonate spectra in the master spectral library.

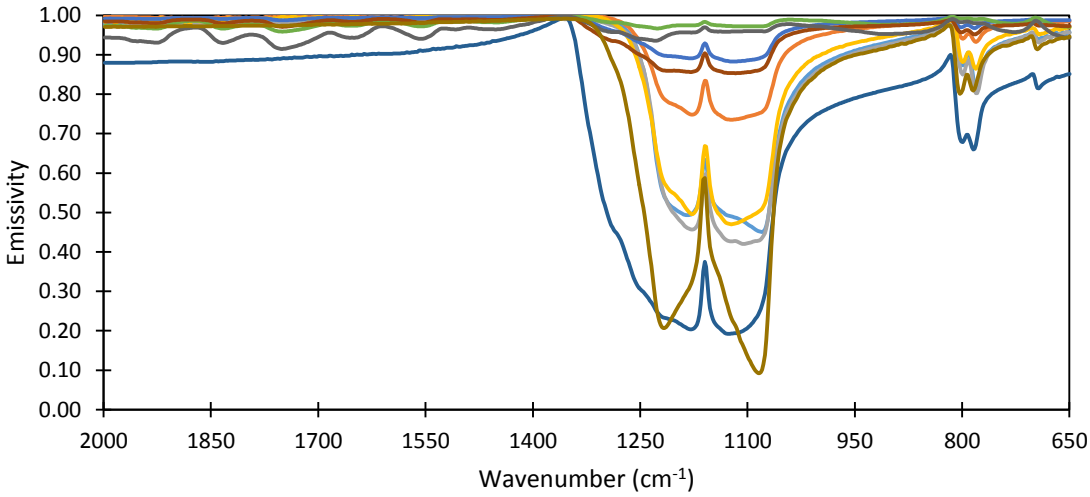

Figure 11: Plot of all quartz spectra in the master spectral library.

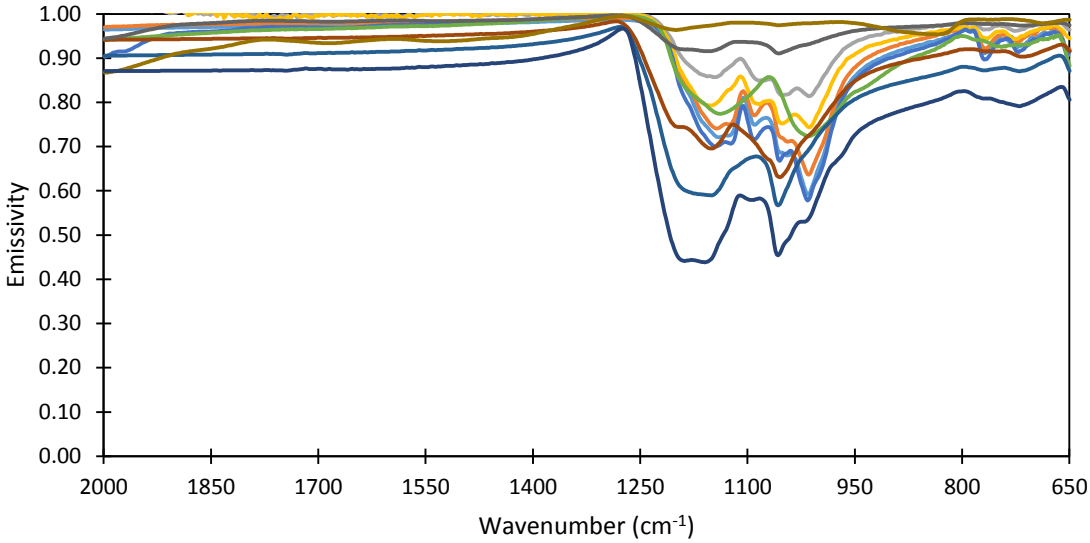

Figure 12: Plot of all K-feldspar spectra in the master spectral library.

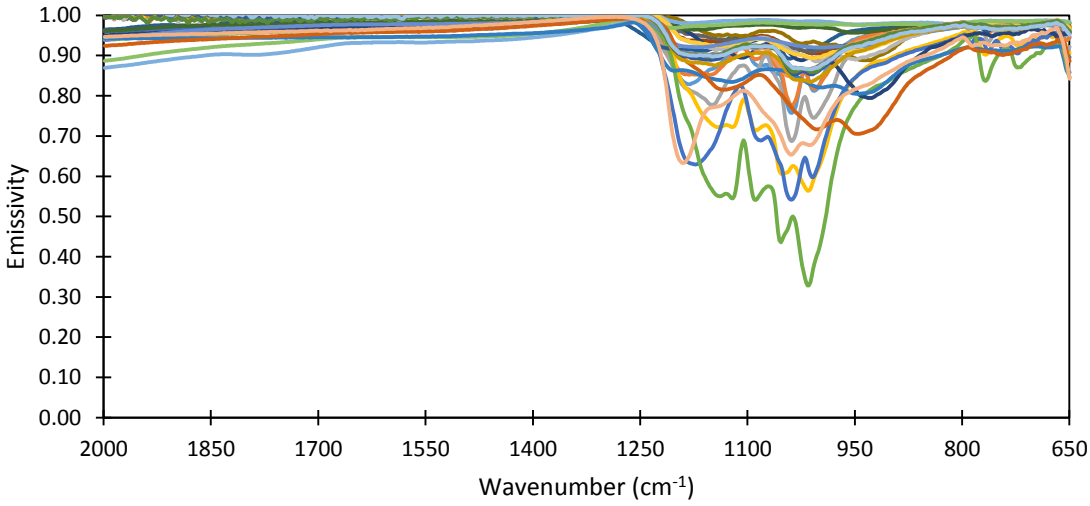

Figure 13: Plot of all plagioclase spectra in the master spectral library.

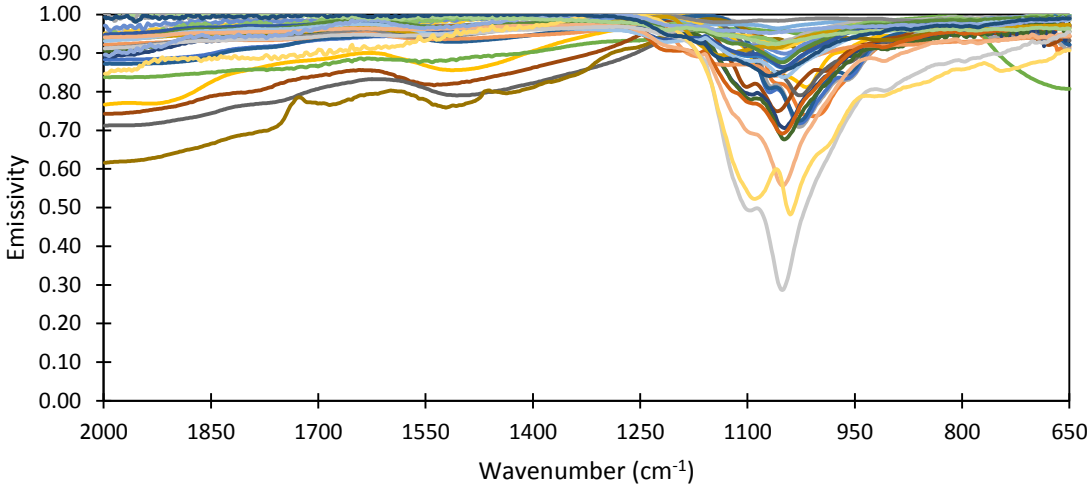

Figure 14: Plot of all phyllosilicate spectra in the master spectral library.

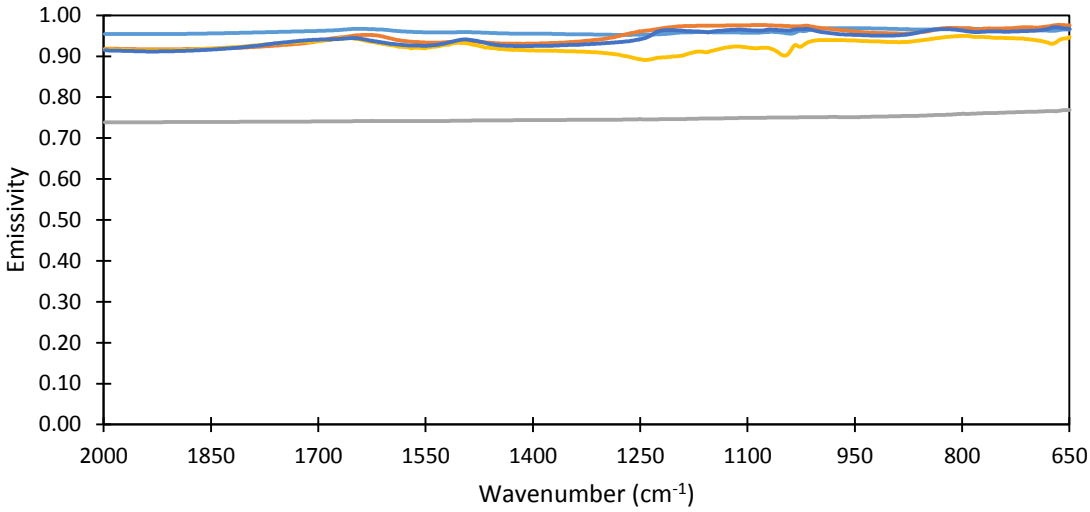

Figure 15: Plot of all sulfide spectra in the master spectral library.

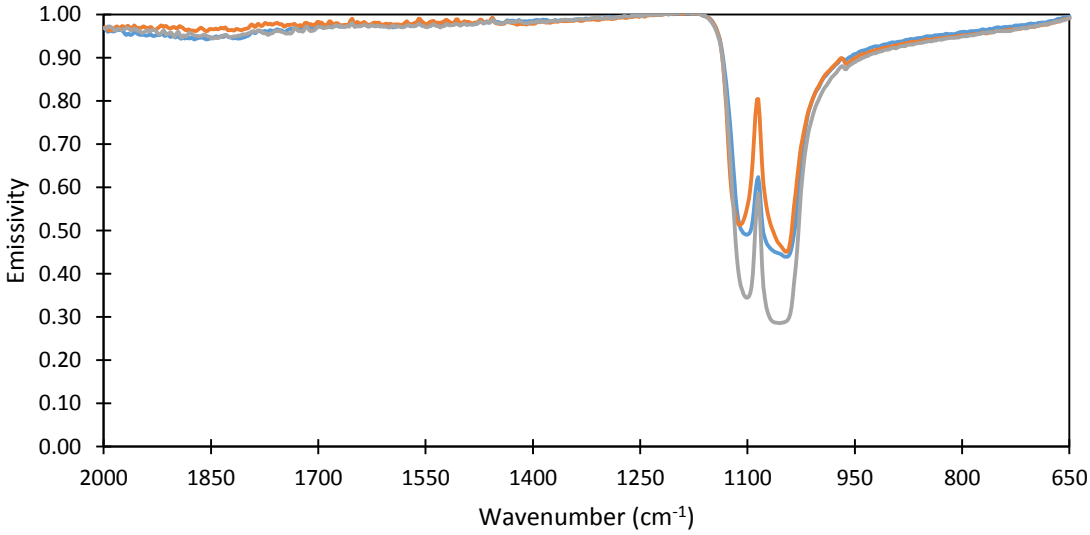

Figure 16: Plot of all phosphate spectra in the master spectral library.

c. Data Conversion

Volumetric proportions of sample components derived from the XRD data provided by Chesapeake Energy is presented in Table 2. Original weight percent data is provided in Appendix B. There was very little change in abundances after converting to volume percentages. However, pyrite decreased by nearly half for all the measurements. All other minerals increased on average of less than one percent. Figure 17 shows the converted abundances plotted.

Tables 2: Mineral and TOC abundances (vol. %) for the Dulcey BRA 5H based on XRD data.

Sample							
Depth	7409	7413	7416	7421	7425	7429	7434
Sample ID	113	115	117	119	121	123	125
Quartz	30.92	29.85	30.64	23.65	29.62	31.40	30.50
K-Feldspar	0.43	0.11	0.00	0.54	0.86	0.00	0.64
Plagioclase	9.47	10.47	9.38	9.07	9.49	9.46	9.57
TOC	4.01	4.91	3.83	3.66	3.72	3.94	3.54
Apatite	0.28	0.37	0.18	0.28	0.18	0.00	0.28
Pyrite	2.58	2.20	2.42	1.87	2.81	1.92	2.47
Calcite	1.83	1.73	2.75	10.09	1.63	0.61	1.93
Dolomite	2.81	4.93	3.30	10.76	3.78	7.74	2.90
Mixed Layer	5.71	5.04	5.81	3.81	4.19	5.70	5.90
Illite+Mica	41.05	39.57	40.49	35.55	42.88	38.03	42.27
Chlorite	0.92	0.83	1.20	0.74	0.83	1.19	0.00

Sample							
Depth	7437	7442	7445	7450	7453	7497	7500
Sample ID	127	129	131	133B	135B	157	159B
Quartz	25.82	26.34	25.83	27.93	39.47	17.55	26.65
K-Feldspar	0.43	0.22	0.54	0.00	0.00	0.00	0.00
Plagioclase	9.20	11.03	11.24	10.28	11.04	2.71	2.10
TOC	4.12	4.76	5.05	7.27	7.34	0.89	4.29
Apatite	0.18	0.19	0.28	0.38	0.37	0.18	0.00
Pyrite	2.37	3.89	4.01	4.60	3.79	0.60	0.32
Calcite	2.56	1.85	0.52	11.42	6.19	61.30	52.71
Dolomite	14.09	1.08	0.98	1.98	2.55	7.06	4.27
Mixed Layer	4.01	5.97	5.20	3.69	3.95	0.00	0.00
Illite+Mica	37.21	44.67	46.35	32.46	25.28	9.71	9.66
Chlorite	0.00	0.00	0.00	0.00	0.00	0.00	0.00

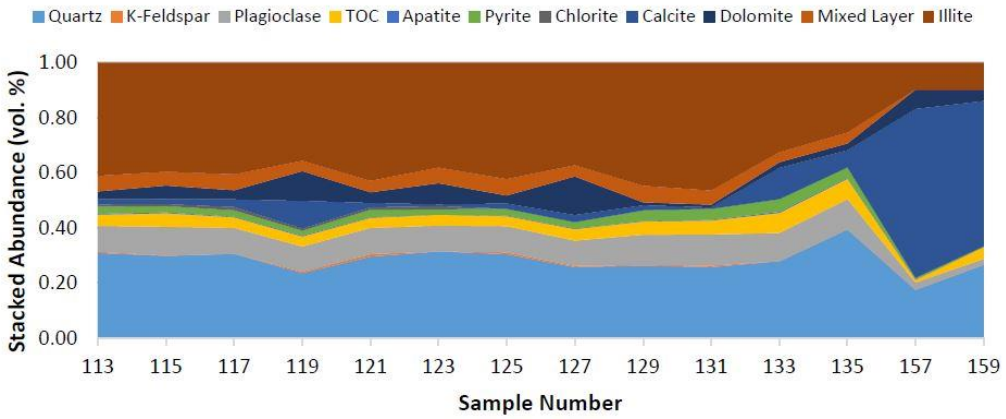

Figure 17: Mineral and TOC abundances (vol. %) for the Dulcey BRA 5H based on XRD data.

d. Forward Mixing

Two different approaches for forward mixing were tested. The first optimized endmembers based on lowest RMS values (producing the RMS Forward-Mixed Library), and the second used the representative Marcellus Formation spectrum (producing the Averaged Shale Library). Both techniques provided varied results. The RMS Forward-Mixed Library is comprised of four spectra that were generated at the OSU Remote Sensing Laboratory, three spectra from the JHU Spectral Library, two from the USGS Digital Spectral Library, and one from ASU TES Laboratory Spectral Library (Appendix A). RMS values from forward mixing using this library range from 1.45% to 3.37%. The lower RMS values are at the upper end (i.e., clay-rich portion) of the core and increase with depth. The Averaged Shale Library is comprised of four spectra that were generated at the OSU Remote Sensing Laboratory, two from the JHU Spectral Library, two from the USGS Digital Spectral Library, and two from the ASU TES Laboratory Spectral Library (Appendix A). Forward mixing using the Averaged Shale Library had RMS errors ranging from 1.03% to 3.13%. The higher RMS values are at the top of the core and decrease with depth (i.e., to the carbonate-rich portion). Tables B1-C1 in the appendices show the comparative results for forward mixing between two different spectral libraries. The RMS Forward-Mixed Library shows better forward modeling for samples 113-119 and 159B, highlighted in green in Table B1, whereas the Averaged Shale Library shows better forward modeling for samples 121-157 (Table C1). Appendix E shows forward mixing results of three characteristic samples, including clay-rich (sample 121), quartz-rich (sample 135b), and carbonate-rich (sample 159b) samples using the RMS Forward-Mixed Library (Figures E1-E3). Appendix F shows the results of forward mixing for the same samples using the Averaged Shale Library (Figure F1-F3).

e. Spectral Unmixing/Deconvolutions

Blind unmixing was run for all sample measurements. The RMS error from the measured spectra ranged from 0.81% to 1.75%. However, the RMS error for mineral abundances relative to the XRD abundances ranged from 10.50% to 21.33%, with a mean of 13.23%. The modeled abundances derived from the full blind unmixing technique are illustrated in Figure 18. The full results table and plot for the blind unmixing can be found in Appendices G-H. The results for the three characteristic samples are plotted in Figures H2-H4, showing the modeled spectra, the measured spectra, and the residual between the two for each of the three samples (samples 121, 135b, and 159b).

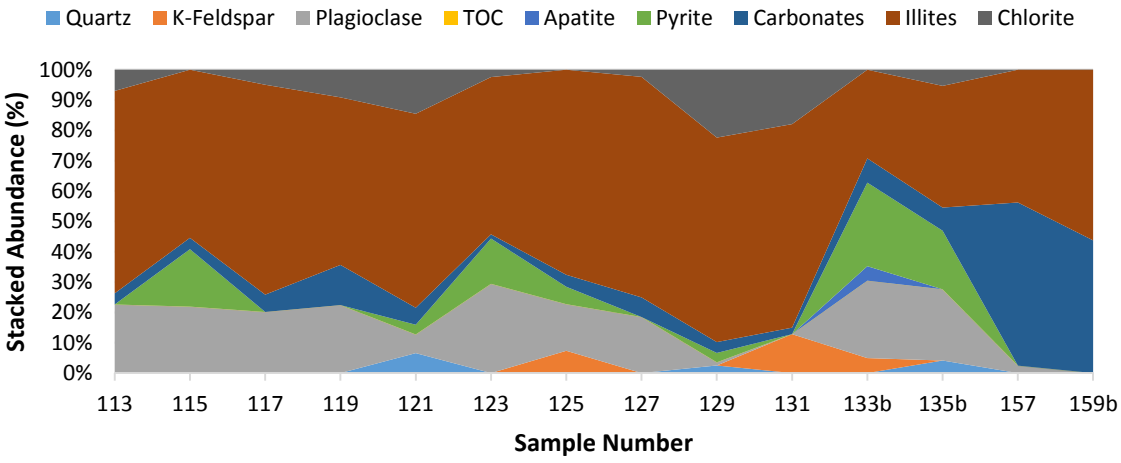

Figure 18: Mineral and TOC abundances (vol. %) resulting from the full blind unmixing.

Unmixing results from using the two forward mixing libraries (RMS Forward-Mixed Library and the Averaged Shale Library) were well outside the XRD results and therefore considered unacceptable.

The Modified Forward-Mixed Library consists of two spectra collected in the OSU Remote Sensing Laboratory, four from the JHU Spectral Library, two spectra from the USGS Digital Spectral Library, and two spectra from the ASU TES Laboratory Spectral Library. The Modified Forward-Mixed Library is illustrated in Figure 19. The mineral abundances found using

this library were much closer than using the previous two methods (blind unmixing and using the two forward mixing libraries). RMS error from the measured spectra ranged from 0.99% to 2.10%. The RMS error from the mineral abundances ranged from 4.49% to 7.94%, with a mean of 6.36%. The data table showing the unmixing results for all samples is located in Appendix I; abundances for the odd samples are plotted in Figure 20 (abundances for entire core plotted in Appendix J1). Results for the three characteristic samples are plotted in Appendices J2-J4 showing the modeled spectra, the measured spectra, and the residual between the two for each of the three samples (samples 121, 135b, and 159b).

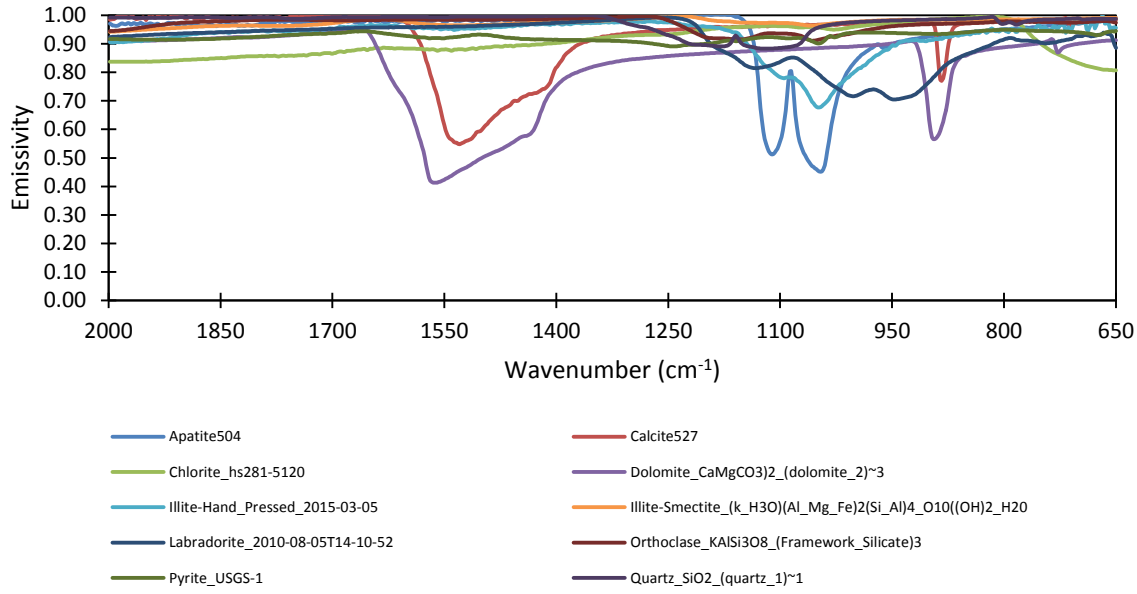

Figure 19: All ten spectra for the Modified Forward-Mixed Library.

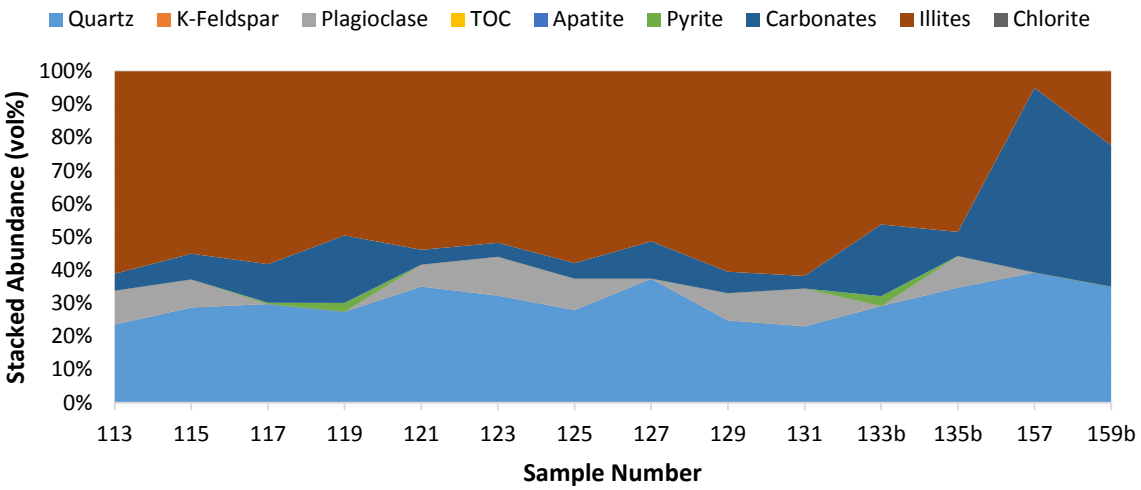

Figure 20: Unmixing results using the Modified Forward-Mixed Library.

The Modified Forward Hand-Picked Library consists of 15 spectra; three spectra generated in the OSU Remote Sensing Laboratory, five from the JHU Spectral Library, three spectra from the USGS Digital Spectral Library, and four spectra from the ASU TES Laboratory Spectral Library (Figure 21). The mineral abundances found using this library were, on average, the closest to the XRD abundances. RMS errors from the measured samples ranged from 0.91% to 2.08%; RMS errors from the mineral abundances ranged from 4.40% to 7.91%, with a mean of 5.72%. The unmixng results for all samples is located in Appendix K. Abundances for odd samples are plotted in Figure 22 (abundances for entire core plotted in Appendices K-L). The results for the three characteristic samples are plotted in Appendices L2-L4 showing the modeled spectra, the measured spectra, and the residual between the two for each of the three samples (samples 121, 135b, and 159b).

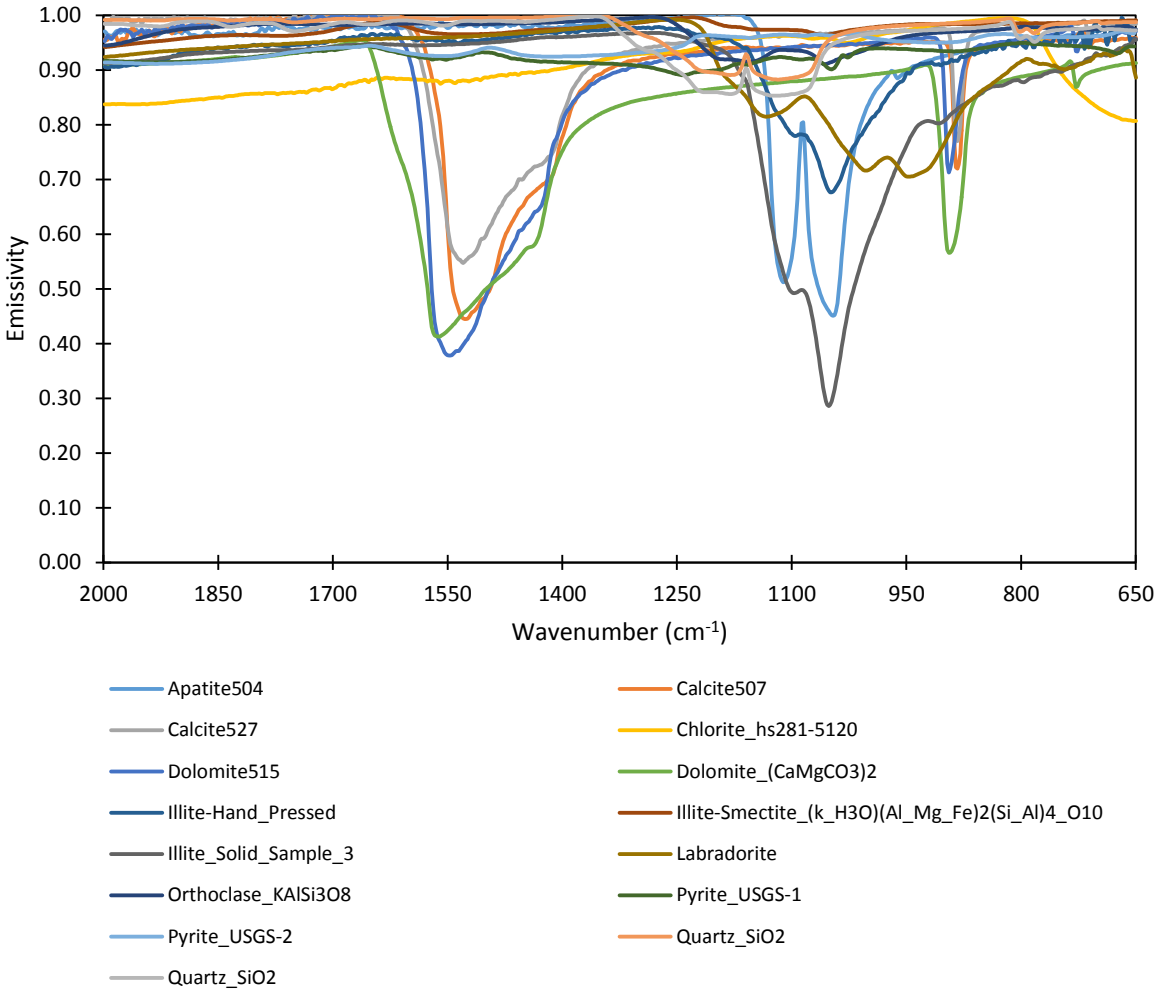

Figure 21: The 15 spectra comprising the Modified Hand-Picked Library.

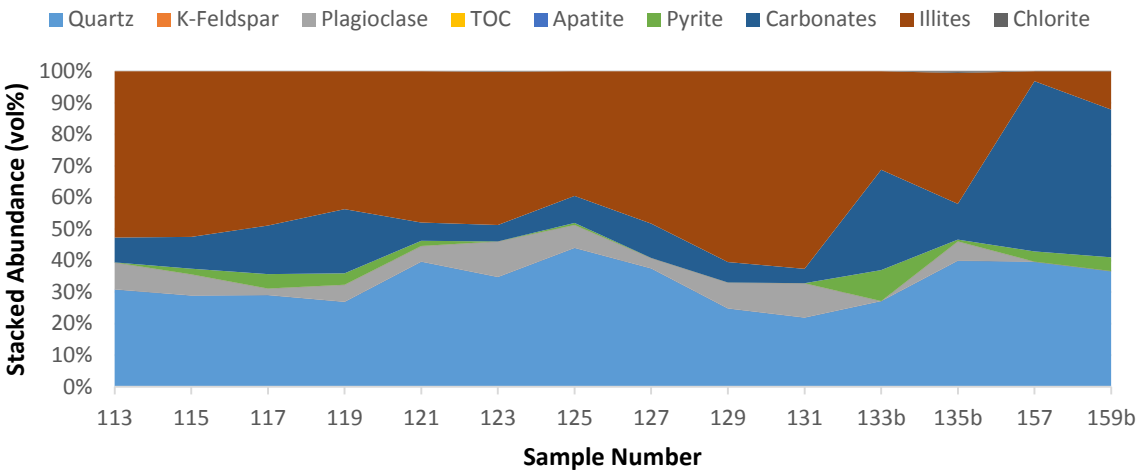

Figure 22: Unmixing results using the Modified Hand-Picked Library, percent abundance on the y-axis, sample number on the x-axis.

CHAPTER V

DISCUSSION

a. Measuring Core

Chesapeake marked areas of about three inches on the core face that were sampled for XRD analysis using their in-house method following Chipera and Bish (2002). As stated in the methods, problems arose while trying to measure the smooth face of the core. Because measurements were taken perpendicular to bedding surfaces, there was a high probability of producing a spectrum that was not representative of the XRD. This is expected due to compositional variation among laminae. Because spectra were taken on pieces of the core that were already broken, it is likely that these pieces broke along bedding planes, which are natural planes of weakness caused by natural alignment of phyllosilicates (Ingram, 1953). If a section is bioturbated, the horizontal arrangement of the clay particles will be disrupted, and the fissility will be diminished (Potter et al., 1980). Because spectra were generated perpendicular to the bedding planes, and the XRD samples are pieces of the core that have been ground and then mixed, it is expected that clay content for the FTIR samples will be higher than measured by XRD. Future work could include a highly descriptive lithologic core description covering the samples used as well as thin section analysis at each sample locality in order to address this issue. To see how close the mineralogic analysis between FTIR spectral unmixing and XRD analysis could get, I would propose taking multiple measurements of a core billet using the FTIR, then

creating an XRD sample of the same billet, and comparing the results. A spectral image could essentially be created by following the methodology from Kruse (1996). Applying the unmixing method demonstrated in this study, a spectral image could be made by creating a gird and taking spectra of each cell. Because the spectrometer spot size is less than 0.1 in (2 mm), the grid sizes could be quite small. This would allow for visualizing mineralogy distribution on a small scale through the core.

b. Endmember Library Compilation

General compositional knowledge of samples prior to analysis of spectra was highly beneficial because it greatly constrained possible endmembers for the spectral library. Although conducting spectral deconvolution without such prior knowledge is common in the remote sensing community and has been successfully implemented by many investigators, the additional constraints available for this study are beneficial for many reasons, including limiting potential spectral matches to components that are geologically reasonable. Online public access is available for all spectral libraries used in this study, apart from spectra generated at the OSU Remote Sensing Laboratory. It's important to know what instrument will be used, how the instrument measures spectra, and what limitations this can or will create. It is preferable to have the mixed spectra (samples for unmixing) and the entire endmember library measured using the same method (i.e. bidirectional reflectance, biconical reflectance, hemispheric reflectance, or emissivity) (Salisbury and Vergo, 1991; Christensen et al., 2000; Clark et al., 2007) and ideally the same intrument. However, this study shows that utilizing spectra generated by different methods if feasible for unmixing.

Through all of the forward mixing, eight spectra from the OSU Remote Sensing Laboratory, five spectra from the John Hopkins University Spectral Library, four spectra from the USGS Digital Spectral Library, and three spectra from the Arizona State University Thermal

Emission Spectroscopy Laboratory Spectral Library were used. Through deconvolution, five spectra from the OSU Remote Sensing Laboratory, nine spectra from the JHU Spectral Library, five spectra from the USGS Digital Spectral Library, and six spectra from the ASU TES Laboratory Spectral Library were used. Which endmember spectra yield the best model results could be due in part to the different methods used to gather the samples, or this could just be caused by spectra variability seen throughout different samples, as illustrated by Figure 23. Spectral variability is brought about by different hand samples (slight variations in crystal lattice, or impurities), grain size, or different instruments and techniques for sampling (Ramsey and Christensen, 1998).

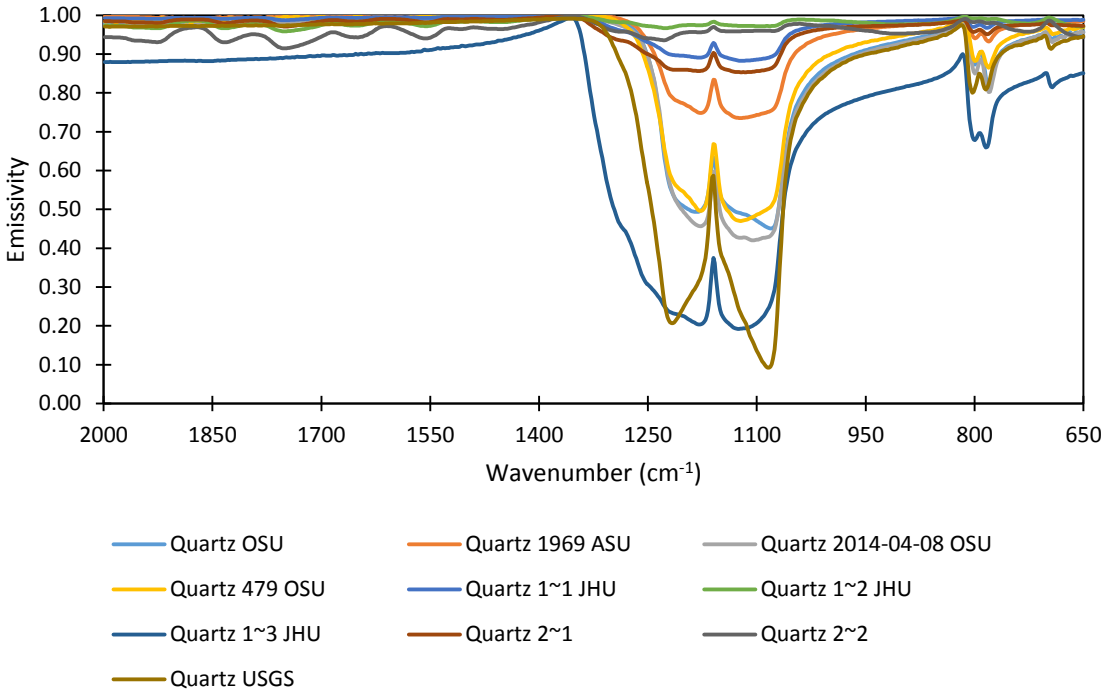

Figure 23: Quartz spectra variability from the four digital spectral libraries.

c. Data Conversion

Conversion of the XRD results provided by Chesapeake Energy from weight percent to volume percent was necessary for comparison to the results generated using FTIR unmixing. The

heavy minerals, such as pyrite and apatite, changed the most (decreasing in percentage by nearly half). This is due to their greater specific gravity. Calculated TOC density ranges from 2.71 to 2.91 g/cm^3 and averaged 2.81 g/ cm^3. There is a slight correlation between TOC values and calculated TOC specific gravity as shown by Figure 24. As organic matter is thermally matured within a sample, secondary porosities can develop within the organic matter (Curtis et al., 2012). More work is needed to see if this correlation is legitimate or is an artifact of the methodology. There are many factors that would need to be taken into account for a future study looking at TOC with FTIR spectroscopy including; the type of kerogen in the core, the dispersion of the organic matter along bedding planes and vertically, and the compaction of layers and organic matter. With additional study, FTIR spectroscopy could potentially provide a faster, nondestructive, more consistent, and more complete approach to characterizing the abundance and thermal maturity of various kerogens than current methods, such as vitrinite reflectance.

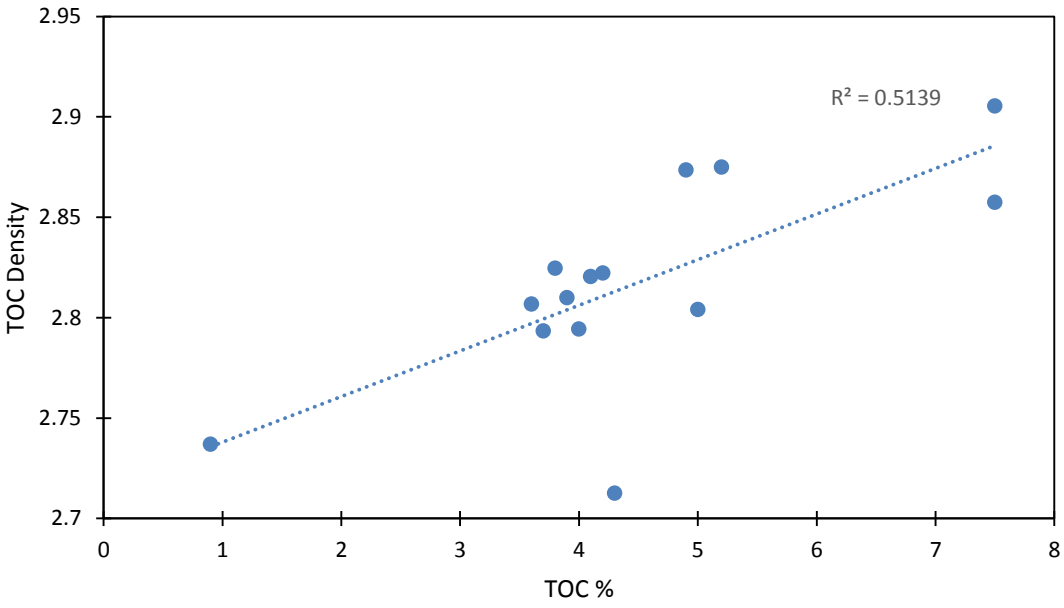

Figure 24: Positive correlation between TOC percent and calculated specific gravity values for TOC, R^2 value of 0.51.

d. Forward Mixing

Problems arose early for the first attempts of picking spectra for forward mixing and it became evident that creating a single forward mixing spectral library was insufficient. The core's composition changes with depth. Of the 14 samples measured, 10 of the samples are clay-rich (main components being illite and an illite/smectite mixed layer; samples 113-121 and 125-133), two of the samples are quartz-rich (quartz abundance >30 wt. %;,samples 123 and 135), and two of the samples are carbonate-rich (main component carbonate; samples 157 and 159). The spectra chosen for forward mixing based on using the lowest RMS error changed for each measured sample. This means that there is a discrepancy of the favorable mineral spectra at each measured sample. The endmember spectra chosen at one sample may not be the best spectra for forward mixing of another sample. This could be brought about by diagenetic alterations as the rock is buried, possible change in the source for detrital components, or as a change in the grain size of minerals in the core (Ramsey and Christensen, 1998), although in some cases it may be influenced by noise in the measured mixed and endmember spectra. Two spectral libraries were created to cover the inconsistency in spectral selection through the core.

e. Spectral Unmixing/Deconvolutions

It was noticed early on while running deconvolutions that the unmixing algorithm has difficulties discerning the difference between calcite and dolomite. However, abundance of carbonate minerals (mainly calcite and dolomite) were much closer to the combined values from the XRD results. This process was also applied to the illite+mica group and the illite/smectite mixed layer. Grouping the illitic clays together was done to help account for the expected higher amounts of clay, caused by measuring fissile layers within the Marcellus Formation. This makes for nine components to be unmixed and accounted for (quartz, k-feldspar group, plagioclase group, TOC, apatite, pyrite, carbonates, illitic clays, and chlorite).

The blind unmixing was modeled after a method utilized by Feely and Christensen (1999) to test unmixing with their master spectral library (116 spectra, 18 minerals and/or components). This method was by far the worst method to use for deconvolution. However, this method produced results faster than any other technique, and therefore could have utility. After the grouping of calcite and dolomite, as well as illitic clays, the averaged RMS error from abundance was 13.44%. This is well outside the expected possible accuracy of the FTIR analysis. Quartz was the mineral with the highest error for this method. This is probably due to the algorithm preferentially selecting other tectosilicates that more closely match the measured spectrum as a whole, rather than trying to fit the spectral features of quartz as seen in Figure 19 (about 1300-1050 cm^{-1}). This is evident by the modeled results of plagioclase, which were often over estimated by 10-20%. The anticipated higher abundances of clays are seen by this method; the over estimations range from 3-35%. Appendix M shows the unmixing results side by side to XRD for the blind method.

As previously stated, attempts at unmixing using the previously created forward mixing libraries (RMS Forward-Mixed Library and the Averaged Shale Library) were unsuccessful. This was caused by high amounts of pyrite being used through every model run. This brought about the modification of the forward mixed libraries. Once a reasonable pyrite was found for unmixing purposes, other minerals were subjected to replacement. This process continued until the Modified Forward-Mixed Library was created. This subset spectral library has the second lowest averaged RMS from abundances at 5.33%. This error is just outside the optimistic unmixing results of five percent. The spectral library created contains ten spectra to match the XRD minerals presented. This does not allow for any spectral variability for each mineral. If a core shows any mineral variability, which is highly likely and seen in the Dulcey BRA 5H, this method will not account for that variability. If the core could be sectioned off by detailed lithologic descriptions and this method was then used for each of the separate facies, then mineral

variability could be taken into account. Just like in the previous method, and as expected, the clay mineral content found using this method was higher than shown by the XRD results for all but one sample. However, the clay mineral abundances generated were much closer than the previous method, averaging 10.59% greater than shown by XRD. Appendix N shows the unmixing results side by side to XRD using the Modified Forward-Mixed Library.

First attempts at creating a hand-picked spectral library for deconvolution by starting with the master library and discarding spectra through unmixing iterations proved ineffective. An unexpected high interplay between spectra used by the algorithm for deconvolution occurred. It was thought exchanging spectra of a mineral through iterations would not affect the weight, or strength, of the other mineral components, however this was incorrect. Spectra were discarded from the library based on their unreasonable abundances found by deconvolution. At first, spectra were excluded four to five at a time depending on abundances returned. After a couple dozen iterations, minerals needed for efficient unmixing were not available. Each time this was encountered, the method was reverted to the beginning, with the original master spectral library, and fewer minerals were excluded after each iteration. A high interplay among spectra was observed. After a single mineral's spectrum was thrown out of the library, all components abundances would change, not just that mineral's spectrum or abundance. After noting this interplay, a new approach was taken. Instead of beginning with the master library and eliminating spectra based on their abundances, the iterations would begin with the Modified Forward-Mixed Library, and spectra would be added to the library to help account for spectral variability though the core. Once the Modified Hand-Picked Library was created, unmixing results from using the new subset library produced the lowest RMS error from abundances at an average of 4.82%. This value is better than the target 5% RMS error for deconvolution results. Clay minerals were on average over estimated by 6.39%. Appendix O shows the unmixng results side by side to XRD using the Modified Forward-Mixed Library.

The RMS error values for each of the three methods for every mineral are provided in Appendix P. The RMS error from total abundance using each of the three methods is plotted in Figure 25. All three method's RMS increases with depth. This could be caused by an increase in carbonate minerals and the FTIR being unable to differential specific minerals, or it could be caused by errors generated while measuring the core. Quartz abundance in the last two measurements, which are from carbonate-rich strata, are overestimated by nearly ten percent. The carbonate abundance is underestimated by more than ten percent for each of the unmixing methods.

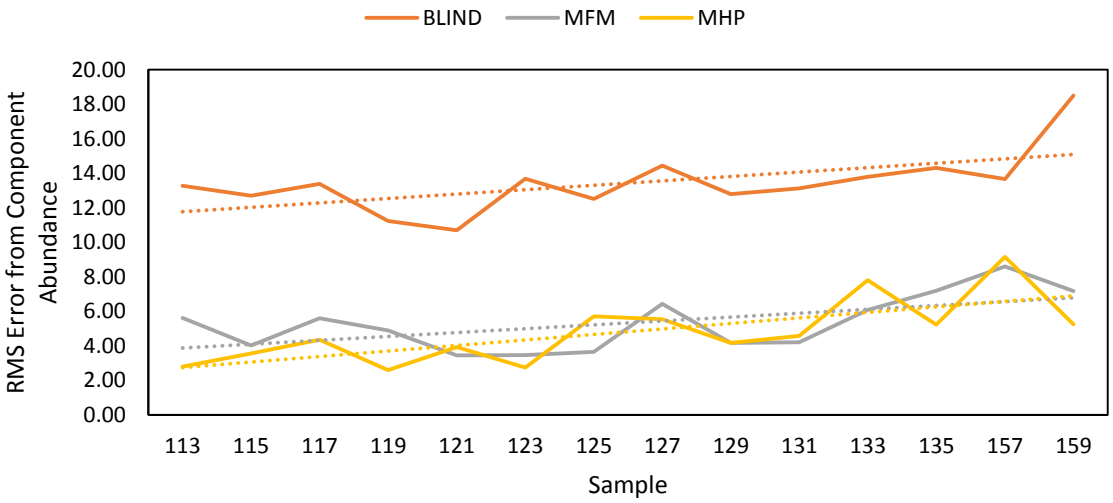

Figure 25: RMS error from component abundances (MFM: Modified Forward-Mixed, MHP: Modified Hand-Picked). Corresponding linear fits indicated as dashed lines.

As each measured spectrum is a linear combination of its components, it was thought at the beginning of this study that finding a spectrum that would account for TOC would be feasible. TOC in the core ranges from 0.89-7.34 vol. %. The plan was to use the residual spectrum between the forward mixed models, or the models created by unmixing, and that of the measured spectra and synthesize a spectrum for TOC. However, after generating the forward mixed models and attempting this method the spectra produced were not meaningful, having wide ranging

emissivity values and many values less than zero. Additionally, TOC spectra calculated for each sample were averaged to limit the influence of noise in the final model TOC spectrum, seen in Figure 26, which still produced an unreasonable result. After finding the average unmixing RMS errors, it became clear it was not going to be possible to create a spectrum for TOC. Synthesizing the XRD data with the FTIR unmixing results provides a rough way to double check the results. Because the two measurements were not taken from the exact same location, as well as the problems presented by measuring perpendicular to bedding planes, the initial technique conceived for calculating a spectrum for TOC was not effective. Future work that generated spectra at exactly the same sampling area as XRD would allow a more comprehensive comparison to construct a spectrum to account for TOC. With variability seen in mineral spectra, it is probable that TOC would exhibit spectral variability just as much, if not more, than minerals do. The varying densities calculated for TOC through the core would support this conclusion. Multiple spectra would have to be produced to account for this variability within a core.

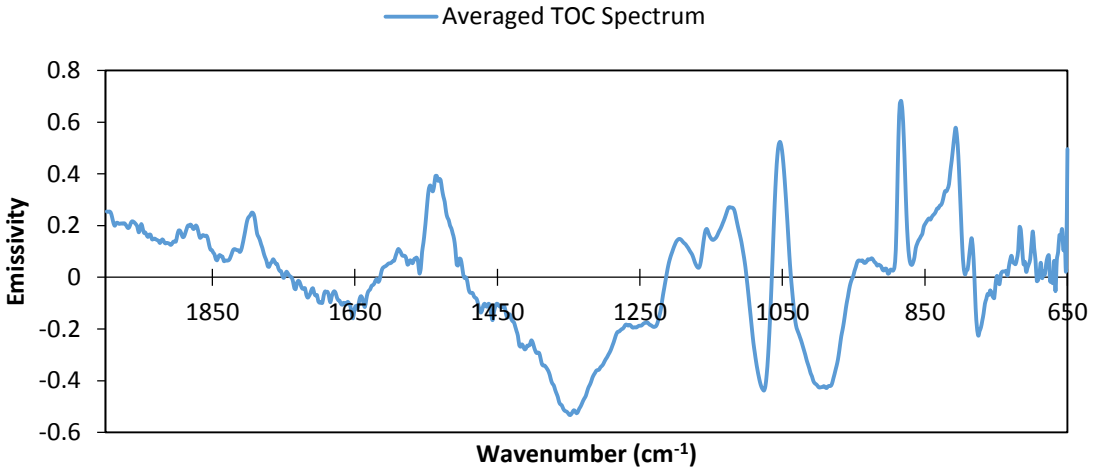

Figure 26: Averaged TOC spectrum for all samples. Calculation was done by utilizing residual spectrum, and the TOC abundance at each data point.

CHAPTER VI

CONCLUSION

a. Endmember Library Compilation

A master spectral library was compiled contained 118 components used for deconvolution. The library includes primary and secondary minerals incorporated in the Marcellus Formation, based on the XRD data supplied by Chesapeake Energy and Potter et al. (1980). The library was built using four sources, three of which have digital access. The most used source (unmixing and mixing) was the JHU Spectral library, second was the spectra generated at the OSU Remote Sensing Library, third was the ASU TES Laboratory Spectral Library, and last was the USGS Digital Spectral Library. Four subset libraries that were used for forward mixing or unmixing were created using spectra from the master library. Differences in these spectral libraries indicate that it is important to consider assumptions going in to compiling spectral endmember libraries, but that it is also important to consider levels of acceptable error in selecting a specific methodology to use.

b. Data Conversion

The provided XRD data were converted from weight percent to volume percent. This was needed to compare results generated by spectral unmixing to XRD results. While converting abundances, calculations were run to find apparent TOC content. The variations seen in density (specific gravity) will likely coincide with spectral variations for TOC content. Overall, the method used to model TOC density produced reasonable results for the measured core.

c. Forward Mixing

Forward mixing showed mineral spectra variation throughout the core. This spectral variability could be due to a change in source for detrital components. As a result, two spectral libraries were created that were later used as starting points for creating unmixing libraries. The comparison between the forward mixing models created using the two forward mixing libraries, and the measured spectra showed that hyperspectral analysis would be possible. Additionally, the importance of the initial forward mixing analyses to constrain the spectral endmember libraries for later deconvolution indicates how important it is to incorporate additional constraints on the FTIR data when available, such as was the case based on availability of XRD data.

d. Spectral Unmixing/Deconvolutions

Three methods, each using a separate spectral library, were tested to analyze a section of the Dulcey BRA 5H core for mineral abundance. The first method, blind unmixing, produced results fastest, but with the highest error of the three methods (average RMS error from abundance 13.44%). The second method used a modified version of the forward mixing libraries (Modified Forward-Mixed Library). This method produced the second lowest RMS error abundances at 5.33%. This method came in second for amount of time needed to build and run samples. This method also does not account for mineral spectral variability. The last method used produced the lowest RMS error from abundance at 4.82%. Using the Modified Hand-Picked library allows the model to account for mineral spectral variability. However this is by far the most time intensive method created. Despite the time investment, tightly constraining the deconvolution approach with the XRD data allows for many additional FTIR measurements to be made with no additional XRD data (as demonstrated with the even numbered samples), essentially allowing for very high resolution studies to be possible on the core for very little additional time and cost. Average RMS error relative to XRD abundances for the best unmixing

technique was under five percent. However, this combined with the variability in sampling regions between the XRD and FTIR make computation of a spectrum for TOC unfeasible. Further work could be done to produce spectra for TOC.

REFERENCES

Adam, H., Harville, D., Meer, D., and Freeman, D., 1988, Rapid Mineral Analysis by Fourier Transform Infrared Spectroscopy: Society of Core Analysts, v. 66, no. 5, p. 677-687.

Adamu, M., 2010, Fourier Transform Infrared Spectroscopic Determination of Shale Minerals in Reservoir Rocks: Nigerian Journal of Basic and Applied Sciences, v. 18, no. 1, p. 35-43.

Arthur, M.A., and Sageman, B.B., 1994, Marine Shales: Depositional Mechanisms and Environments of Ancient Deposits: Annual Review of Earth and Planetary Sciences, v. 22, p. 499-551.

Baldridge, A., Hook, S., Grove, C., and Rivera, G., 2009, The ASTER spectral library version 2.0: Remote Sensing of Environment, v. 113, no. 4, p. 711-715.

Ballard, B.D., 2007, Quantitative Mineralogy of Reservoir Rocks Using Fourier Transform Infrared Spectrscopy, SPE International, Society of Petroleum Engineers.

Brett, C.E., and Baird, G.C., 1996, Middle Devonian Sedimentary Cycles and Sequences in the Northern Appalachian Basin: SPECIAL PAPERS-GEOLOGICAL SOCIETY OF AMERICA, p. 213-242.

Byrnes, J.M., and Byrnes, J.J., 2011, Thermal Infrared Reflectance and Emission for Remote Analysis of Planetary Surfaces: Lunar and Planetary Science Conference, v. 42, p. 2384.

Byrnes, J.M., Ramsey, M.S., King, P.L., and Lee, R.J., 2007, Thermal Infrared Reflectance and Emission Spectroscopy of Quartzofeldspathic Glasses: Geophysical Research Letters, v. 34, no. 1.

Chipera, S.J., and Bish, D.L., 2002, FULLPAT: a full-pattern quantitative analysis program for X-ray powder diffraction using measured and calculated patterns: Journal of Applied Crystallography, v. 35, no. 6, p. 744-749.

Christensen, P.R., Bandfield, J.L., Hamilton, V.E., Howard, D.A., Lane, M.D., Piatek, J.L., Ruff, S.W., and Stefanov, W.L., 2000, A thermal emission spectral library of rock‐forming minerals: Journal of Geophysical Research: Planets (1991‐2012), v. 105, no. E4, p. 9735-9739.

Clark, R.N., Swayze, G.A., Wise, R., Livo, K.E., Hoefen, T.M., Kokaly, R.F., and Sutley, S.J., 2007, USGS Digital Spectral Library splib06a, US Geological Survey Reston, VA.

Curtis, M.E., Cardott, B.J., Sondergeld, C.H., and Rai, C.S., 2012, Development of organic porosity in the Woodford Shale with increasing thermal maturity: International Journal of Coal Geology, v. 103, p. 26-31.

Feely, K.C., and Christensen, P.R., 1999, Quantitative Compositional Analysis Using Thermal Emission Spectroscopy: Application to igneous and metamorphic rocks: Journal of Geophysical Research: Planets (1991–2012), v. 104, no. E10, p. 24195-24210.

Hapke, B., 1993, Theory of reflectance and emittance spectroscopy, Cambridge University Press.

Herron, M.M., Matteson, A., and Gustavson, G., 1997, Dual-Range FT-IR Mineralogy and the Analysis of Sedimentary Formations, Society of Core Analysts: Calgary, SCA, v. 9729, p. 7-10.

Herron, M.M., Matteson, A., and Supp, M., 1998, Method for Quantitative Analysis of Earth Samples: Patent, Google Patents.

Hunt, J.M., and Turner, D.S., 1953, Determination of mineral constituents of rocks by infrared spectroscopy: Analytical Chemistry, v. 25, no. 8, p. 1169-1174.

Incropera, F.P., Lavine, A.S., and DeWitt, D.P., 2011, Fundamentals of Heat and Mass Transfer, John Wiley & Sons.

Ingram, R.L., 1953, Fissility of Mudrocks: Geological Society of America Bulletin, v. 64, no. 8, p. 869-878.

Johnson, P.E., Smith, M.O., and Adams, J.B., 1992, Simple Algorithms for Remote Determination of Mineral Abundances and Particle Sizes from Reflectance Spectra: Journal of Geophysical Research: Planets (1991–2012), v. 97, no. E2, p. 2649-2657.

Klein, C., Dutrow, B., and Dana, J.D., 2002, Manual of Mineral Science, Wiley New York.

Kruse, F., 1996, Identification and mapping of minerals in drill core using hyperspectral image analysis of infrared reflectance spectra: International journal of remote sensing, v. 17, no. 9, p. 1623-1632.

Kruse, F., Lefkoff, A., Boardman, J., Heidebrecht, K., Shapiro, A., Barloon, P., and Goetz, A., 1993, The spectral image processing system (SIPS)—interactive visualization and analysis of imaging spectrometer data: Remote sensing of environment, v. 44, no. 2, p. 145-163.

Lash, G.G., and Engelder, T., 2011, Thickness trends and sequence stratigraphy of the Middle Devonian Marcellus Formation, Appalachian Basin: Implications for Acadian foreland basin evolution: AAPG bulletin, v. 95, no. 1, p. 61-103.

Lewan, M., 1978, Laboratory classification of very fine grained sedimentary rocks: Geology, v. 6, no. 12, p. 745-748.

Loucks, R.G., Reed, R.M., Ruppel, S.C., and Hammes, U., 2012, Spectrum of pore types and networks in mudrocks and a descriptive classification for matrix-related mudrock pores: AAPG bulletin, v. 96, no. 6, p. 1071-1098.

Lundegard, P.D., and Samuels, N.D., 1980, Field classification of fine-grained sedimentary rocks: Journal of Sedimentary Research, v. 50, no. 3.

Lyon, R., and Burns, E.A., 1963, Analysis of rocks and minerals by reflected infrared radiation: Economic Geology, v. 58, no. 2, p. 274-284.

Lyon, R.J.P., 1963, Evaluation of infrared spectrophotometry for compositional analysis of lunar and planetary soils: Washington, D.C., National Aeronautics and Space Administration.

Lyon, R.J.P., Tuddenham, W.M., and Thompson, C.S., 1959, Quantitative mineralogy in 30 minutes: Economic Geology, v. 54, no. 6, p. 1047-1055.

Matteson, A., and Herron, M.M., 1993, Quantitative mineral analysis by Fourier transform infrared spectroscopy, in Society of Core Analysts Conference.

Milici, R.C., and Swezey, C., 2006, Assessment of appalachian basin oil and gas resources: Devonian shale-middle and upper paleozoic total petroleum system, US Department of the Interior, US Geological Survey.

Nicodemus, F.E., 1965, Directional reflectance and emissivity of an opaque surface: Applied optics, v. 4, no. 7, p. 767-773.

Piatek, J., and Moersch, J., 2006, A strategy for atmospheric correction of THEMIS infrared data, in 37th Annual Lunar and Planetary Science Conference, p. Abstract 1158.

Picard, M.D., 1971, Classification of fine-grained sedimentary rocks: Journal of Sedimentary Research, v. 41, no. 1.

Potter, P.E., Maynard, J.B., and Pryor, W.A., 1980, Final report of special geological, geochemical, and petrological studies of the Devonian shales in the Appalachian Basin: Cincinnati Univ., OH (USA). HN Fisk Lab. of Sedimentology.

Potter, P.E., Maynard, J.B., and Pryor, W.A., 1980, Sedimentology of Shale; Study Guide and Reference Source, New York, Springer-Verlag.

Ramsey, M.S., 1996, Quantitative analysis of geological surfaces: a deconvolution algorithm for midinfrared remote sensing data, Arizona State University, 276 p.

Ramsey, M.S., and Christensen, P.R., 1998, Mineral abundance determination: Quantitative deconvolution of thermal emission spectra: Journal of Geophysical Research: Solid Earth (1978–2012), v. 103, no. B1, p. 577-596.

Roberts, D.A., Gardner, M., Church, R., Ustin, S., Scheer, G., and Green, R., 1998, Mapping chaparral in the Santa Monica Mountains using multiple endmember spectral mixture models: Remote Sensing of Environment, v. 65, no. 3, p. 267-279.

Salisbury, J.W., and Vergo, N., 1991, Infrared (2.1-25 um) spectra of minerals, Johns Hopkins University Press.

Salisbury, J.W., Wald, A., and D'Aria, D.M., 1994, Thermal‐infrared remote sensing and Kirchhoff's law: 1. Laboratory measurements: Journal of Geophysical Research: Solid Earth (1978‐2012), v. 99, no. B6, p. 11897-11911.

Sondergeld, C.H., and Rai, C.S., 1993, A new exploration tool: Quantitative core characterization: pure and applied geophysics, v. 141, no. 2-4, p. 249-268.

Wessman, C.A., Bateson, C.A., and Benning, T.L., 1997, Detecting fire and grazing patterns in tallgrass prairie using spectral mixture analysis: Ecological Applications, v. 7, no. 2, p. 493-511.

APPENDICES

Appendix A: Full list of spectra in the master spectral library. Minerals included in subset libraries indicated as RMS Forward-Mixed (RFM), Averaged Shale (AS), Modified Forward-Mixed (MFM), and Modified Hand-Picked (MHP) Libraries.

Albite_2014-03-06T21-25-27 (AS)
Albite_2014-03-06T21-27-36
Albite_2014-03-06T21-30-05
Albite_NaAlSi3O8
Albite454
Albite483
Albite560
Andesine0434
Andesine0561
Anorthite_2010-08-05T13-58-44
Anorthite_CaAl2Si2O8
Anorthite_CaAl2Si2O8
Anorthite564
Anorthoclase485
Apatite501 (RFM, AS)
Apatite504 (MFM, MHP)
Apatite506
Calcite_2014-03-06
Calcite_2014-03-06T21-34-26
Calcite_2014-03-06T21-37-06 (RFM)
Calcite_CaCO3_(calcite_1)~2
Calcite_CaCO3_(calcite_1)~3
Calcite_CaCO3_(calcite_1)~4
Calcite_CaCO3_(calcite_1)~5
Calcite507 (MHP)
Calcite508
Calcite509
Calcite519
Calcite521
Calcite527 (AS, MFM, MHP)
Chlorite_hs179-4703
Illite_Solid_Sample_2010-03-31T12-58-1
Chlorite_hs179-4703 (RFM, AS)
Chlorite_hs197-4759
Chlorite_hs281-5120 (MFM, MHP)
Chlorite_smr13-4862
Chlorite_smr13-4932
Chlorite_smr13-4999
Chlorite_smr13-5063
Chlorite1_2014-04-16T20-37-19
Chlorite466
Dolomite_1-2_2014-04-08T18-57-51 (AS)
Dolomite_1-2_2014-04-08T19-04-51
Dolomite_CaMgCO3)2_(1)~1
Dolomite_CaMgCO3)2_(1)~2
Dolomite_CaMgCO3)2_(1)~3
Dolomite_CaMgCO3)2_(2)~1
Dolomite_CaMgCO3)2_(2)~2
Dolomite_CaMgCO3)2_(2)~3 (MFM, MHP)
Dolomite_CaMgCO3)2_(3)~1
Dolomite_CaMgCO3)2_(3)~2
Dolomite_CaMgCO3)2_(3)~3
Dolomite2_2014-04-08T19-01-53
Dolomite515 (MHP)
Dolomite516 (RFM)
Dolomite517
Dolomite518
Dolomite528
Illite_(K_H3O)(Al_Mg_Fe)2(Si_Al)4O10
Illite_(K_H3O)(Al_Mg_Fe)2(Si_Al)4O10
Illite_31mm_disc_2010-03-31T12-54-05
Illite_Cambrian_Shale_2014-03-05T21-17
Illite_Cambrian_Shale2_2014-03-05T21-1
Oligoclase472

Illite_Solid_Sample_3_2010-03-31T13-05 (MHP)
Illite2133
Illite596
Illite-Hand_Cranked
Illite-Hand_Pressed (RFM, AS, MFM, MHP)
IllitePellet_2010-08-04T10-15-26
IlliteRock_2010-08-04T11-55-56
Illite-Smectite_(k_H3O)(Al_Mg_Fe)1 (MFM, MHP)
Illite-Smectite_(k_H3O)(Al_Mg_Fe)2 (RFM, AS)
Illite-Smectite_layer2375
Illite-Smectite_layer2377
Kspar_STD_2010-02-07T17-18-36
Kspar_STD_face
Labradorite_(NaCa)Al(AlSi)Si2O8
Labradorite_(NaCa)Al(AlSi)Si2O8
Labradorite_(NaCa)Al(AlSi)Si2O8
Labradorite_2010-08-05 (RFM, MFM, MHP)
Labradorite486
Labradorite562
Microcline_2010-08-05T14-25-25
Microcline468
Microcline481
Muscovite449
Oligoclase_2010-08-05T13-31-29
Oligoclase450
Oligoclase476
Oligoclase492
Oligoclase493
Orthoclase_2010-08-05T14-34-25 (AS)
Orthoclase_KAlSi3O8(1)
Orthoclase_KalSi3O8(2)
Orthoclase_KalSi3O8(3) (RFM, MFM, MHP)
Orthoclase_KalSi3O8(4)
Orthoclase_KalSi3O8(5)
Pyrite_FeS2_(pyrite_1)
Pyrite_FeS2_(pyrite_1)~2
Pyrite_FeS2_(pyrite_1)~3
Pyrite_USGS-1 (AS, MFM, MHP)
Pyrite_USGS-2 (RFM, MHP)
Quartz
Quartz_1969
Quartz_2014-04-08T17-37-09
Quartz_2014-04-08T17-39-32
Quartz_479
Quartz_SiO2_(quartz_1)~1 (AS, MFM, MHP)
Quartz_SiO2_(quartz_1)~2
Quartz_SiO2_(quartz_1)~3
Quartz_SiO2_(quartz_2)~1 (RFM, MHP)
Quartz_SiO2_(quartz_2)~2
Quartz_USGS

Appendix B: Original XRD data provided by Chesapeake Energy.

Well Name	Dulcey BRA 5H						
Sample Depth	7409.16	7413.06	7416.3	7420.76	7424.82	8428.8	7433.7
Sample	113	115	117	119	121	123	125
Quartz	29.7	28.7	29.4	22.7	28.4	30.2	29.3
K-Feldspar	0.4	0.1	0	0.5	0.8	0	0.6
Plagioclase	9.3	10.3	9.2	8.9	9.3	9.3	9.4
TOC	4.1	5	3.9	3.7	3.8	4	3.6
Apatite	0.3	0.4	0.2	0.3	0.2	0	0.3
Pyrite	4.7	4	4.4	3.4	5.1	3.5	4.5
Calcite	1.8	1.7	2.7	9.9	1.6	0.6	1.9
Dolomite	2.9	5.1	3.4	11.1	3.9	8	3
TOTAL	53.1	55.2	53.2	60.6	53.1	55.6	52.6
CLAY FRACTION							
ILLITE/SMECTITE	6.0	5.3	6.1	4.0	4.4	6.0	6.2
Illite + Mica	40.0	38.6	39.4	34.6	41.7	37.1	41.2
Chlorite	1.0	0.9	1.3	0.8	0.9	1.3	0.0
TOTAL	47.0	44.8	46.8	39.4	47.0	44.4	47.4
GRAND TOTAL	100.1	100.0	100.0	100.0	100.1	100.0	100.0

Sample Depth	7436.8	7441.58	7444.86	7449.54	7453.22	7497.18	7500.38
Sample	127	129	131	133	135	157	159
Quartz	24.7	25	24.5	26.3	37.4	17.1	26.1
K-Feldspar	0.4	0.2	0.5	0	0	0	0
Plagioclase	9	10.7	10.9	9.9	10.7	2.7	2.1
TOC	4.2	4.9	5.2	7.5	7.5	0.9	4.3
Apatite	0.2	0.2	0.3	0.4	0.4	0.2	0
Pyrite	4.3	7	7.2	8.2	6.8	1.1	0.6
Calcite	2.5	1.8	0.5	11	6	61.1	52.8
Dolomite	14.5	1.1	1	2	2.6	7.4	4.5
TOTAL	59.7	50.8	50	65.3	71.6	90.4	90.4
CLAY FRACTION							
ILLITE/SMECTITE	4.2	6.2	5.4	3.8	4.1	0.0	0.0
Illite + Mica	36.1	43.0	44.6	31.0	24.3	9.6	9.6
Chlorite	0.0	0.0	0.0	0.0	0.0	0.0	0.0
TOTAL	40.3	49.2	50.0	34.8	28.4	9.6	9.6
GRAND TOTAL	100.0	100.0	100.0	100.1	100.0	100.0	100.0

Table C1: RMS Forward-Mixed results (vol. %). Values highlighted in green indicate lower RMS errors for samples modeled using the RMS Forward-Mixed Library relative to the Averaged Shale Library; values highlighted in red indicate higher RMS errors.

Sample ID	113	115	117	119	121	123	125
Quartz	30.92	29.85	30.64	23.65	29.62	31.40	30.50
K-Feldspar	0.43	0.11	0.00	0.54	0.86	0.00	0.64
Plagioclase	9.47	10.47	9.38	9.07	9.49	9.46	9.57
Apatite	0.28	0.37	0.18	0.28	0.18	0.00	0.28
Pyrite	2.58	2.20	2.42	1.87	2.81	1.92	2.47
Calcite	1.83	1.73	2.75	10.09	1.63	0.61	1.93
Dolomite	2.81	4.93	3.30	10.76	3.78	7.74	2.90
Mixed Layer	5.71	5.04	5.81	3.81	4.19	5.70	5.90
Illite/Mica	41.05	39.57	40.49	35.55	42.88	38.03	42.27
Chlorite	0.92	0.83	1.20	0.74	0.83	1.19	0.00
RMS	0.01786	0.01451	0.01788	0.02784	0.01272	0.01288	0.01592

Sample ID	127	129	131	133B	135B	157	159B
Quartz	25.82	26.34	25.83	27.93	39.47	17.55	26.65
K-Feldspar	0.43	0.22	0.54	0.00	0.00	0.00	0.00
Plagioclase	9.20	11.03	11.24	10.28	11.04	2.71	2.10
Apatite	0.18	0.19	0.28	0.38	0.37	0.18	0.00
Pyrite	2.37	3.89	4.01	4.60	3.79	0.60	0.32
Calcite	2.56	1.85	0.52	11.42	6.19	61.30	52.71
Dolomite	14.09	1.08	0.98	1.98	2.55	7.06	4.27
Mixed Layer	4.01	5.97	5.20	3.69	3.95	0.00	0.00
Illite/Mica	37.21	44.67	46.35	32.46	25.28	9.71	9.66
Chlorite	0.00	0.00	0.00	0.00	0.00	0.00	0.00
RMS	0.01482	0.01612	0.01439	0.03191	0.03366	0.02188	0.02786

Appendix D: Forward-mixing results based on using the Averaged Shale Library (Table D1). Values highlighted in green indicate lower RMS errors for samples modeled using the Averaged Shale Library relative to the RMS Forward-Mixed Library; values highlighted in red indicate higher RMS errors.

Table D1: Representative Shale results (vol. %).

Sample ID	113	115	117	119	121	123	125
Quartz	30.92	29.85	30.64	23.65	29.62	31.40	30.50
K-Feldspar	0.43	0.11	0.00	0.54	0.86	0.00	0.64
Plagioclase	9.47	10.47	9.38	9.07	9.49	9.46	9.57
Apatite	0.28	0.37	0.18	0.28	0.18	0.00	0.28
Pyrite	2.58	2.20	2.42	1.87	2.81	1.92	2.47
Calcite	1.83	1.73	2.75	10.09	1.63	0.61	1.93
Dolomite	2.81	4.93	3.30	10.76	3.78	7.74	2.90
Mixed Layer	5.71	5.04	5.81	3.81	4.19	5.70	5.90
Illite/Mica	41.05	39.57	40.49	35.55	42.88	38.03	42.27
Chlorite	0.92	0.83	1.20	0.74	0.83	1.19	0.00
RMS	0.01951	0.01455	0.01803	0.02879	0.01034	0.01158	0.01424

Sample ID	127	129	131	133B	135B	157	159B
Quartz	25.82	26.34	25.83	27.93	39.47	17.55	26.65
K-Feldspar	0.43	0.22	0.54	0.00	0.00	0.00	0.00
Plagioclase	9.20	11.03	11.24	10.28	11.04	2.71	2.10
Apatite	0.18	0.19	0.28	0.38	0.37	0.18	0.00
Pyrite	2.37	3.89	4.01	4.60	3.79	0.60	0.32
Calcite	2.56	1.85	0.52	11.42	6.19	61.30	52.71
Dolomite	14.09	1.08	0.98	1.98	2.55	7.06	4.27
Mixed Layer	4.01	5.97	5.20	3.69	3.95	0.00	0.00
Illite/Mica	37.21	44.67	46.35	32.46	25.28	9.71	9.66
Chlorite	0.00	0.00	0.00	0.00	0.00	0.00	0.00
RMS	0.01399	0.01431	0.01261	0.02854	0.0288	0.02146	0.03134

Appendix E: Example forward-mixing results using the RMS Forward-Mixed Library (Figures E1-E3).

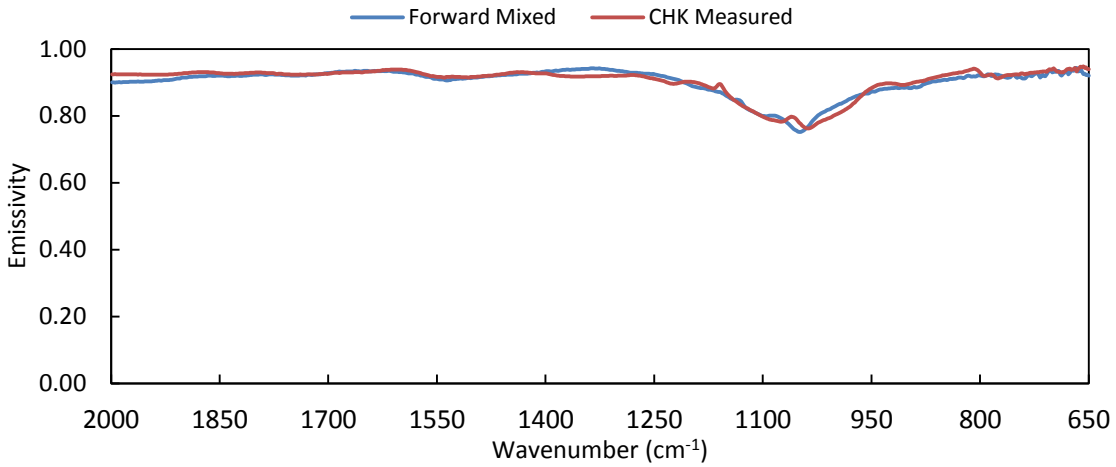

Figure E1: Sample 121 (clay rich) forward-mixing result using the RMS Forward-Mixed Library. Red line shows spectrum measured directly from the core. The blue line shows the spectrum generated by forward mixing. RMS error is 1.27%.

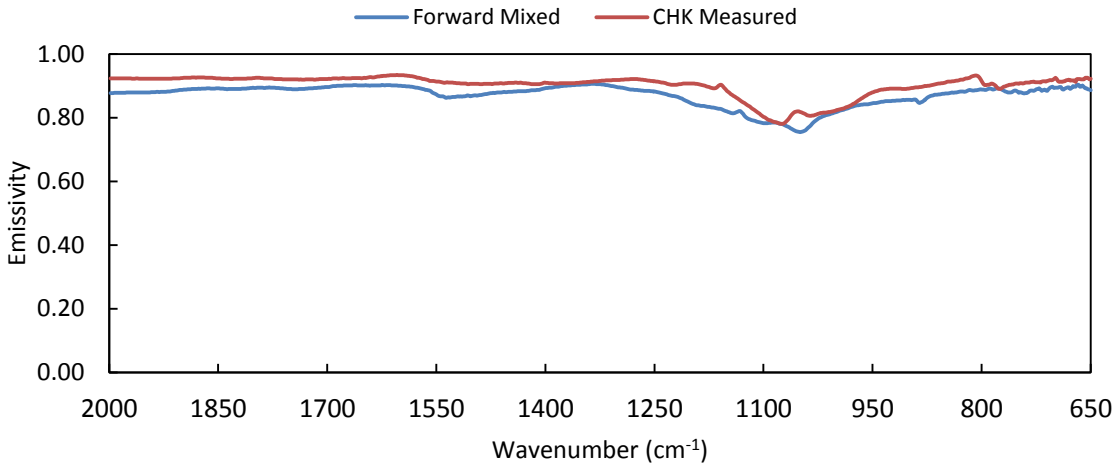

Figure E2: Sample 135b (quartz rich) forward-mixing result using the RMS Forward-Mixed Library. Red line shows spectrum measured directly from the core. The blue line shows the spectrum generated by forward mixing. RMS error of 3.37%.

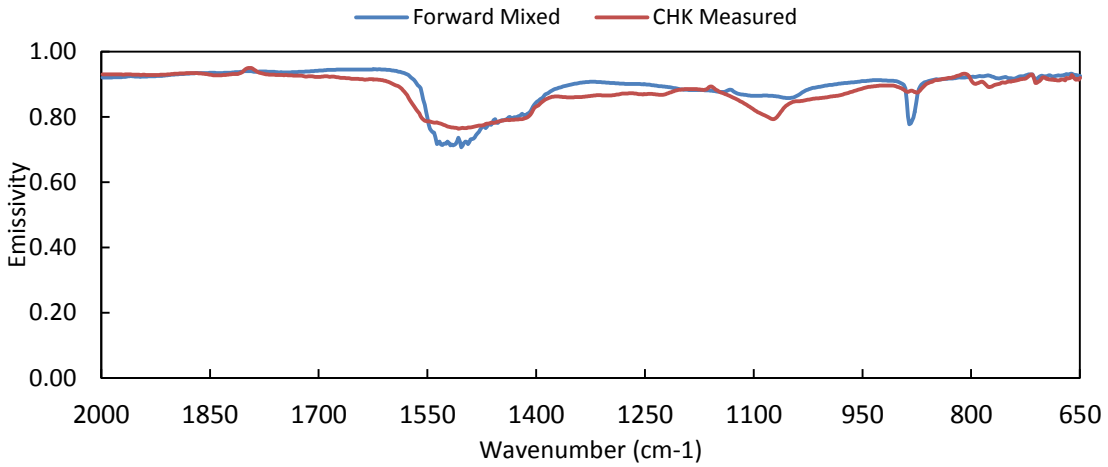

Figure E3: Sample 159b (carbonate rich) forward-mixing result using the RMS Forward-Mixed Library. Red line shows spectrum measured directly from the core. The blue line shows the spectrum generated by forward mixing. RMS error of 2.79%.

Appendix F: Example forward-mixing result using the Averaged Shale Library (Figures F1-F3).

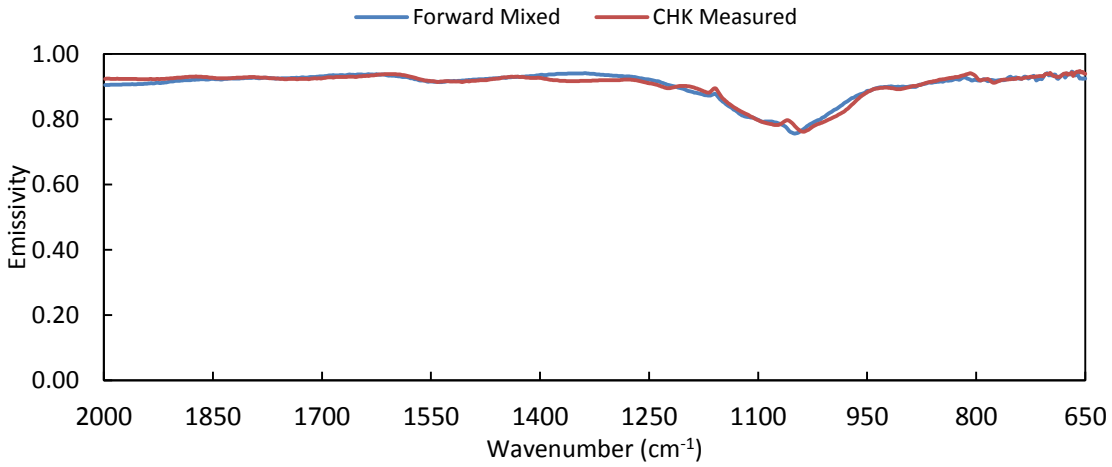

Figure F1: Sample 121 (clay rich) forward-mixing result using the Averaged Shale Library. Red line shows spectrum measured directly from the core. The blue line shows the spectrum generated by forward mixing. RMS error of 1.03%.

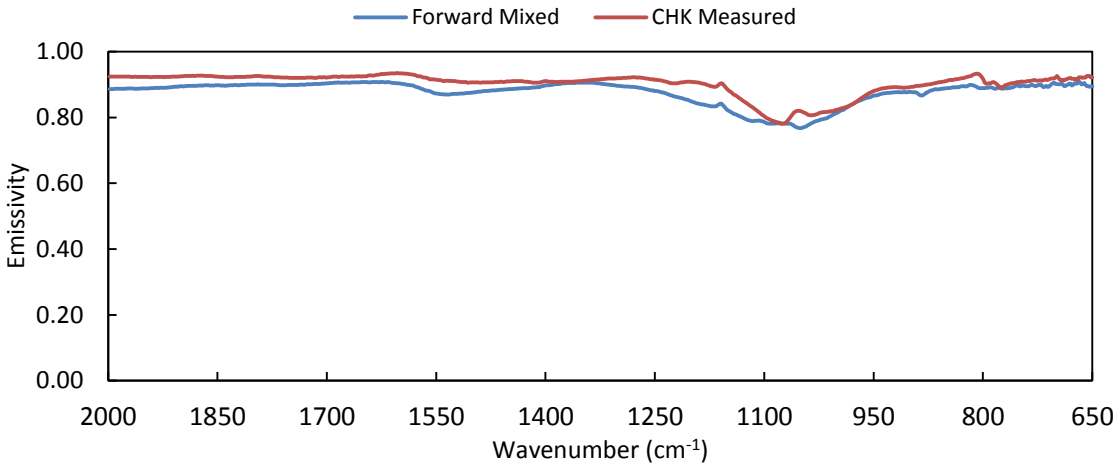

Figure F2: Sample 135b (quartz rich) forward-mixing result using the Averaged Shale Library. Red line shows spectrum measured directly from the core. The blue line shows the spectrum generated by forward mixing. RMS error of 2.88%.

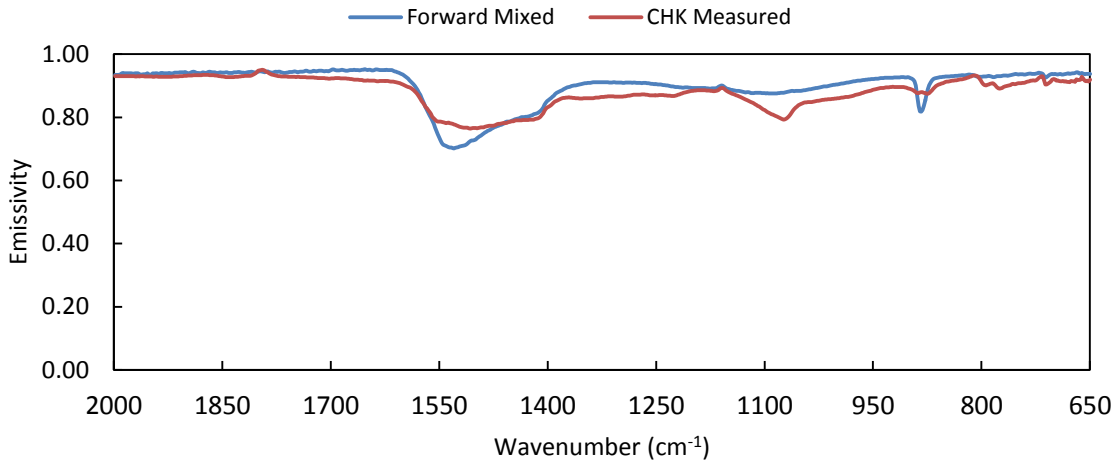

Figure F3: Sample 159b (carbonate rich) forward-mixing result using the Averaged Shale Library. Red line shows spectrum measured directly from the core. The blue line shows the spectrum generated by forward mixing. RMS error of 3.13%.

Appendix G: Tabular results using the full blind unmixing method.

Sample Depth	7409.16		7413.06		7416.3		7420.76		7424.82		8428.8		7433.7
Sample ID	113	114	115	116b	117	118	119	120b	121	122b	123	124	125
Quartz	0	0	0	0	0	0	0	0	6.57	0	0	0	0
K-Feldspar	0	16.75	0	0	0	7.48	0	0	0	12.84	0	0	7.34
Plagioclase	22.6	0	21.9	0	20.13	12.33	22.4	8.62	6.15	3.39	29.41	30.78	15.37
TOC	0	0	0	0	0	0	0	0	0	0	0	0	0
Apatite	0	0	0	0	0	0	0	0	0	0	0	0	0
Pyrite	0	0	18.93	11.92	0	18.4	0	12.3	3.21	10.95	14.92	0	5.74
Calcite	3.68	9.08	3.38	0	5.73	8.32	13.25	10.12	0	0	0	6.54	3.95
Dolomite	0	0	0.37	0	0	0	0	0	5.6	0	1.39	0	0
Illite/Smectite	0	0	0	0	0	0	0	0	0	0	0	0	0
Illite + Mica	66.73	57.85	55.43	67.57	69.18	53.47	55.24	68.96	63.94	66.98	51.84	55.14	67.6
Chlorite	6.99	16.31	0	20.51	4.96	0	9.12	0	14.53	5.84	2.43	7.55	0
RMSE	0.012	0.012	0.0109	0.0094	0.0115	0.0132	0.0178	0.0141	0.0087	0.0075	0.0081	0.0108	0.0094

Sample Depth		7436.8		7441.58		7444.86		7449.54		7453.22	7497.18		7500.38
Sample ID	126	127	128	129	130	131	132	133b	134	135b	157	158c	159b
Quartz	0	0	0	2.5	0	0	0	0	8.34	4.13	0	20.21	0
K-Feldspar	0	0	18.84	0	0	12.82	0	4.93	0	0	0	0	0
Plagioclase	23.52	18.46	1.71	1.05	27.85	0	31.8	25.52	0	23.47	2.45	0	0
TOC	0	0	0	0	0	0	0	0	0	0	0	0	0
Apatite	0	0	0	0	0	0	0	4.77	0	0	0	0	0
Pyrite	0	0	18.41	3.08	0	0	19.98	27.54	15.86	19.32	0	13.22	0
Calcite	2.69	4.39	9.28	3.36	3.02	2.15	7.03	7.99	43.97	7.63	41.47	17.66	14.38
Dolomite	1.94	2.09	2.53	0.22	0.51	0	0	0	16.43	0	12.3	8.53	29.36
Illite/Smectite	0	0	0	0	0	0	0	0	0	0	0	0	0
Illite + Mica	63.88	72.7	31.58	67.42	62.35	67.1	19.84	29.24	15.39	40.11	43.76	40.37	56.26
Chlorite	7.95	2.36	17.65	22.38	6.26	17.94	21.35	0	0	5.33	0	0	0
RMSE	0.0094	0.0085	0.0085	0.0084	0.0129	0.0085	0.0116	0.0133	0.0098	0.0093	0.014	0.0114	0.0175

Appendix H: Results using the full blind unmixing method. Figure H1 shows the unmixing results for all samples measured. Figures H2-H4 show the plots for the models created by deconvolution, the measured spectrum, and the residual between the two.

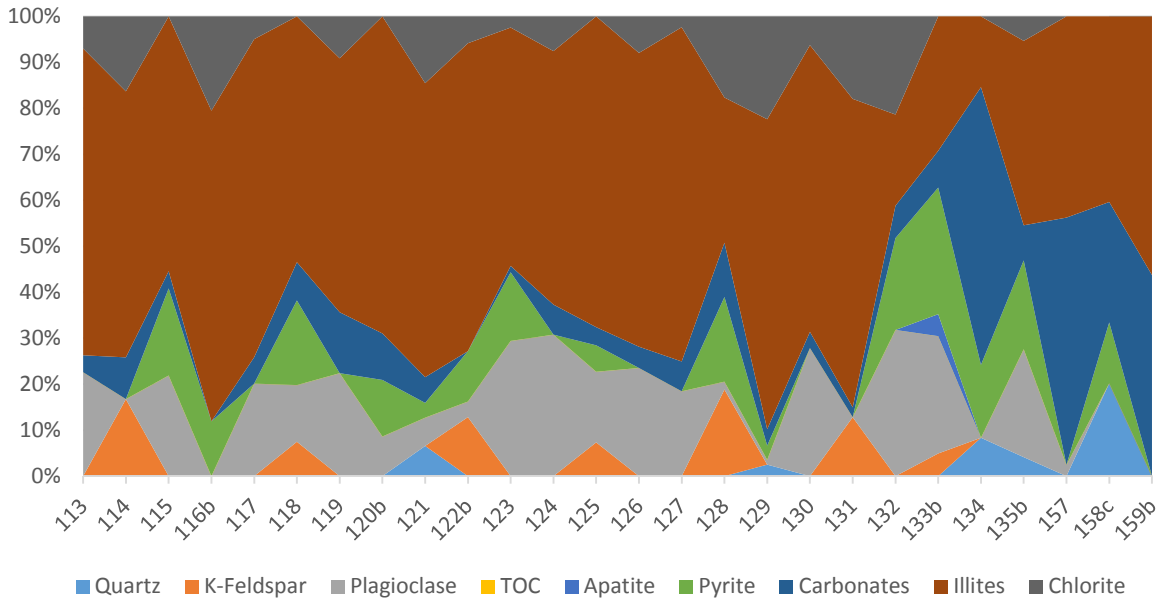

Figure H1: Unmixing results for the all samples measured.

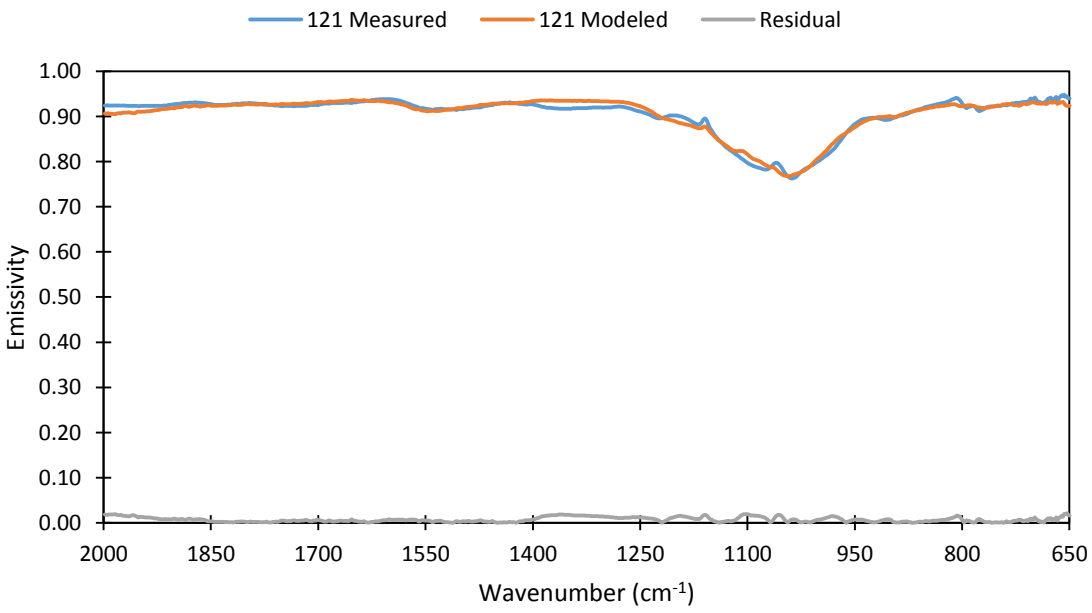

Figure H2: Sample 121 measured and modeled spectra using the full blind unmixing technique.

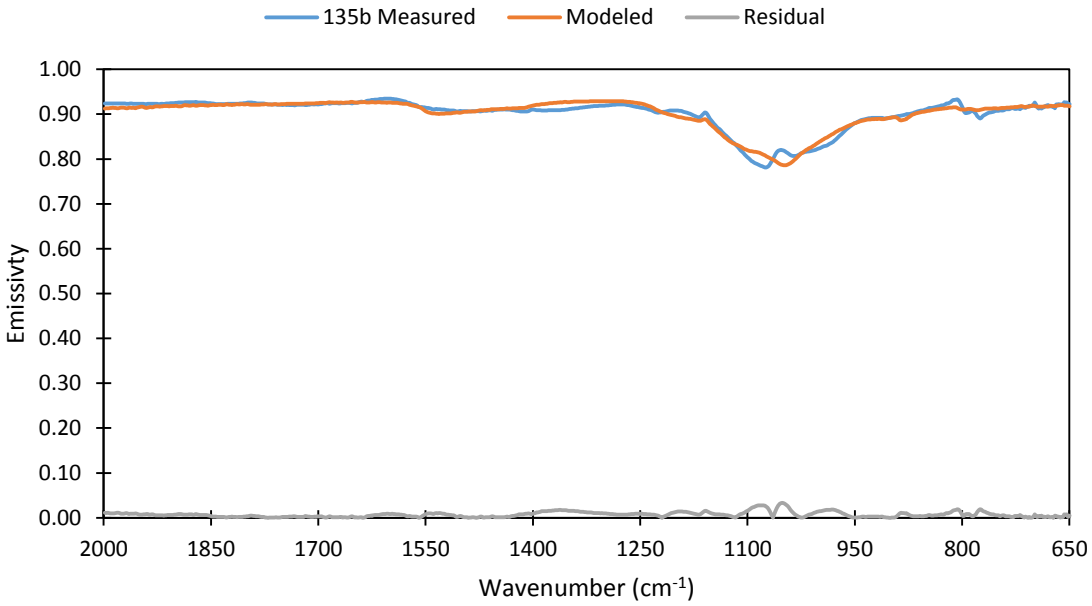

Figure H3: Sample 135b measured and modeled spectra using the full blind unmixing technique.

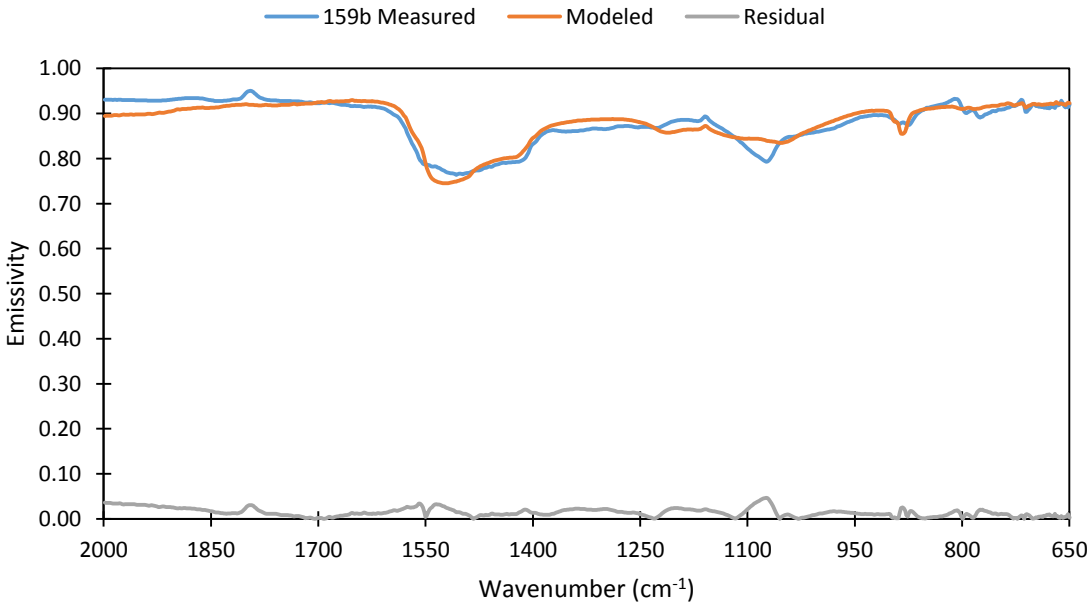

Figure H4: Sample 159b measured and modeled spectra using the full blind unmixing technique.

Appendix I: Tabular results using the Modified Forward-Mixing library for deconvolution.

Sample Depth	7409.16		7413.06		7416.3		7420.76		7424.82		8428.8		7433.7
Sample ID	113	114	115	116b	117	118	119	120b	121	122b	123	124	125
Quartz	23.6	27.11	28.75	20.57	29.76	30.07	27.5	35.14	35.04	33.36	32.31	26.27	27.97
K-Feldspar	0	0	0	0	0	0	0	0	0	0	0	0	0
Plagioclase	10.21	8.85	8.44	0	0	0	0	0	6.62	3.46	11.72	10.58	9.46
TOC	0	0	0	0	0	0	0	0	0	0	0	0	0
Apatite	0	0	0	0	0	0	0	0	0	0	0	0	0
Pyrite	0	0	0	3.49	0.4	0	2.61	7.52	0	0	0	0	0
Calcite	5.08	13.6	7.77	1.88	11.65	13.37	20.35	23.42	4.47	2.89	4.21	11.14	4.69
Dolomite	0	0	0	0	0	0	0	0	0	0	0	0	0
Illite/Smectite	0	0	0	0	0	0	0	0	0	0	0	0	0
Illite + Mica	61.12	50.44	55.05	74.06	58.19	56.56	49.54	33.92	53.87	60.29	51.76	52	57.88
Chlorite	0	0	0	0	0	0	0	0	0	0	0	0	0
RMSE	0.0139	0.0153	0.0123	0.0124	0.0125	0.0164	0.021	0.017	0.0108	0.0092	0.01	0.0123	0.0146

Sample Depth		7436.8		7441.58		7444.86		7449.54		7453.22	7497.18		7500.38
Sample ID	126	127	128	129	130	131	132	133b	134	135b	157	158c	159b
Quartz	29.44	37.44	15.7	24.83	16.28	23.04	4.36	29.19	5.24	34.74	39.31	60.32	35.07
K-Feldspar	0	0	0	0	0	0	0	0	0	0	0	0	0
Plagioclase	7.62	0	10.33	8.22	13.35	11.41	0	0	0	9.52	0	0	0
TOC	0	0	0	0	0	0	0	0	0	0	0	0	0
Apatite	0	0	0	0	0	0	0	0	0	0	0	0	0
Pyrite	0	0	0	0	0	0	0	2.95	0	0	0	0	0
Calcite	9.88	10.37	20.86	6.47	4.17	3.79	15.3	21.64	91.94	7.27	53.81	22.45	38.96
Dolomite	0	0.87	0	0	0	0	0	0	0	0	1.86	3.84	3.61
Illite/Smectite	0	0	0	0	0	0	0	0	0	0	0	0	0
Illite + Mica	53.06	51.32	53.11	60.48	66.19	61.76	80.34	46.22	2.82	48.47	5.02	13.39	22.36
Chlorite	0	0	0	0	0	0	0	0	0	0	0	0	0
RMSE	0.0107	0.0099	0.0101	0.0112	0.0139	0.0117	0.0154	0.016	0.0212	0.0113	0.0127	0.0173	0.0172

Appendix J: Results using the Modified Forward-Mixing library for deconvolution. Figure J1 shows the unmixing results for all samples measured. Figures J2-J4 show the plots for the models created by deconvolution, the measured spectrum, and the residual between the two.

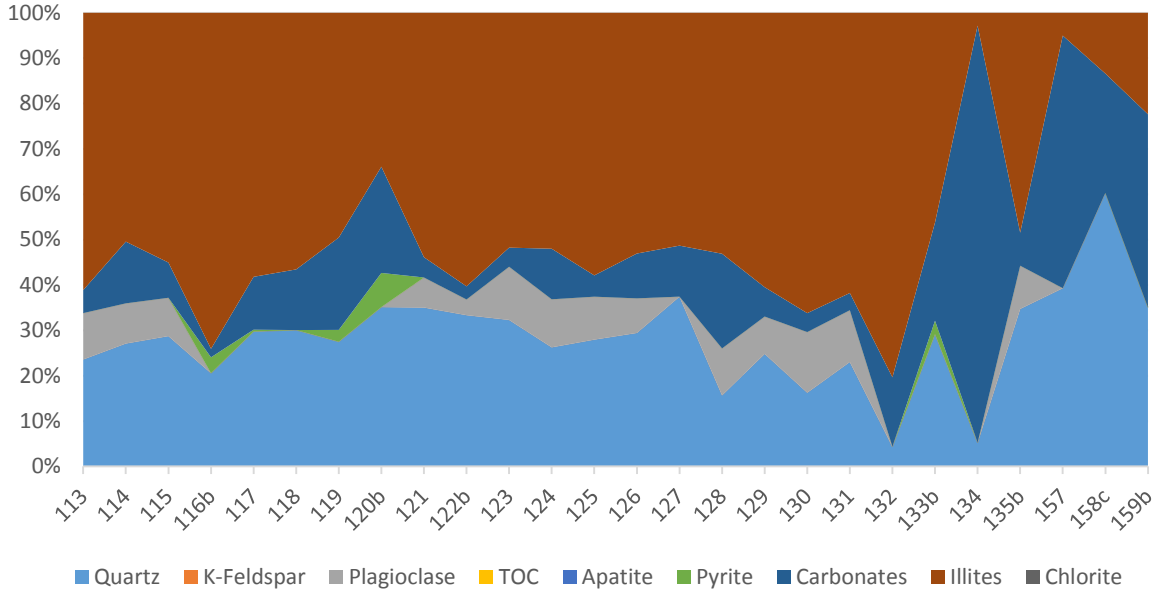

Figure J1: Charted results for all samples using the Modified Forward-Mixed Library for deconvolution.

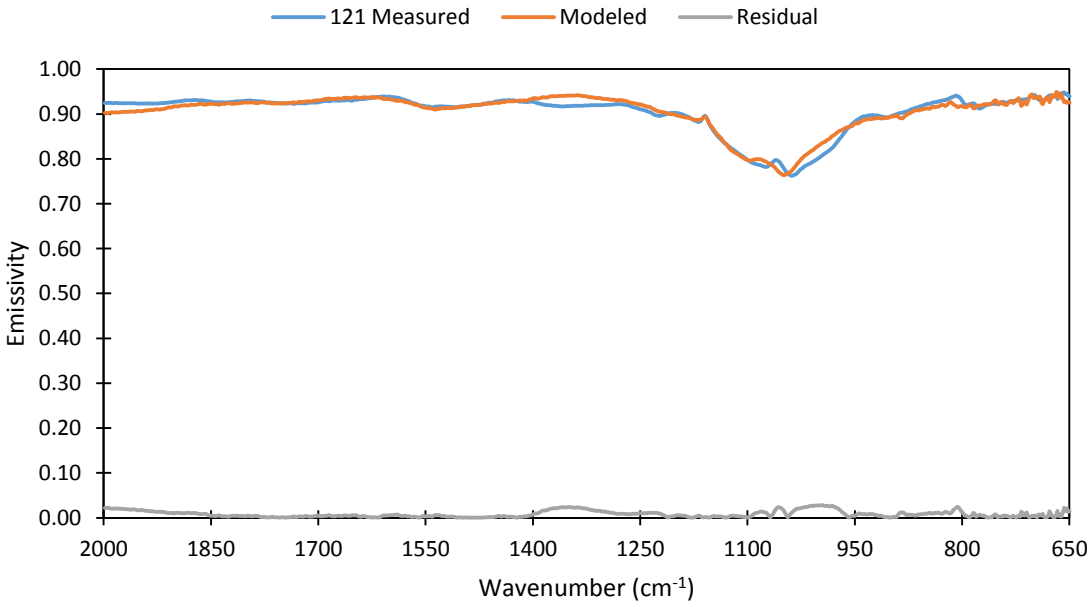

Figure J2: Sample 121 measured and modeled using the Modified Forward-Mixed Library.

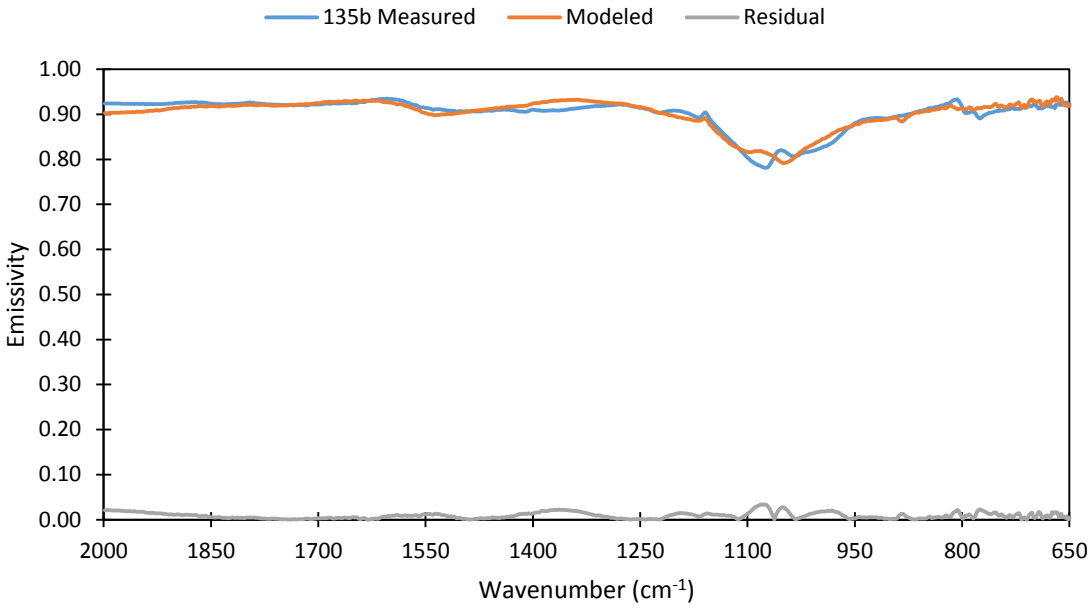

Figure J3: Sample 135b measured and modeled using the Modified Forward -Mixed Library.

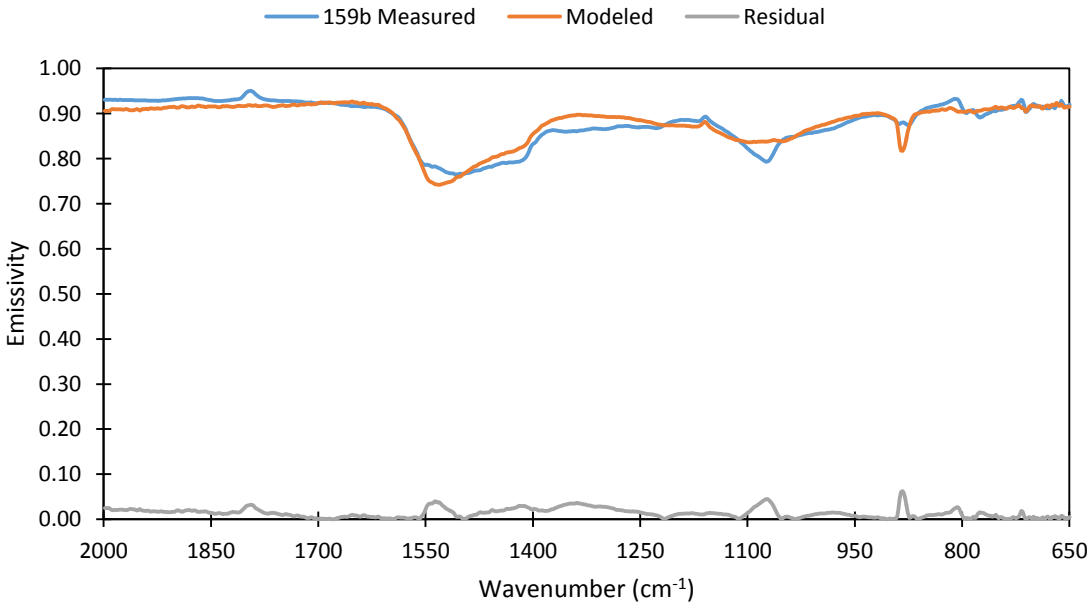

Figure J4: Sample 159b measured and modeled using the Modified Forward-Mixed Library.

Appendix K: Tabular results using the Modified Hand-Picked library for deconvolution

Sample Depth	7409.16		7413.06		7416.3		7420.76		7424.82		8428.8		7433.7
Sample ID	113	114	115	116b	117	118	119	120b	121	122b	123	124	125
Quartz	30.88	27.64	28.93	20.46	29.07	29.33	26.93	35.14	39.67	33.66	34.81	24.7	44.03
K-Feldspar	0	0	0	0	0	0	0	0	0	0	0	0	0
Plagioclase	8.52	6.26	6.7	1.5	2.06	2.69	5.4	0	4.95	2.65	11.26	9.36	7.26
TOC	0	0	0	0	0	0	0	0	0	0	0	0	0
Apatite	0	0	0	0	0	0	0	0	0	0	0	0	0
Pyrite	0.02	5.09	1.78	3.77	4.57	6.22	3.62	7.52	1.64	0.7	0	3.71	0.63
Calcite	7.88	20.64	10.09	2	15.4	20.57	20.34	23.42	5.79	2.99	4.91	15.75	8.56
Dolomite	0	0	0	0	0	0	0	0	0	0	0.3	0	0
Illite/Smectite	0	0	0	0	0	0	0	0	0	0	0	0	0
Illite + Mica	52.71	40.35	52.5	72.27	48.91	41.18	43.71	33.92	47.95	59.99	48.56	46.47	39.51
Chlorite	0	0	0	0	0	0	0	0	0	0	0.18	0	0
RMSE	0.0124	0.014	0.0116	0.0124	0.0117	0.015	0.0208	0.017	0.0101	0.0092	0.0091	0.0113	0.0109

Sample Depth		7436.8		7441.58		7444.86		7449.54		7453.22	7497.18		7500.38
Sample ID	126	127	128	129	130	131	132	133b	134	135b	157	158c	159b
Quartz	29.95	37.52	12.19	24.83	24.85	21.93	4.54	27.16	16.92	39.98	39.66	64.32	36.68
K-Feldspar	0	0	0	0	0	0	0	0	0	0	0	0	0
Plagioclase	6.4	3.3	9.54	8.22	0	10.88	13.88	0	0	6.09	0	0	0
TOC	0	0	0	0	12.3	0	0	0	0	0	0	0	0
Apatite	0	0	0	0	0	0	0	0	0	0	0	0	0
Pyrite	0.48	0	0.85	0	0	0	1.98	9.81	0	0.56	3.23	0	4.34
Calcite	11.76	8.61	26.58	6.47	6.97	4.56	15.69	31.8	72.45	11.34	49.82	16.34	43.61
Dolomite	0	2.28	0	0	0	0	0	0	9.12	0	4.17	9.67	3.24
Illite/Smectite	0	0	0	0	0	0	0	0	0	0	0	0	0
Illite + Mica	51.4	48.29	50.84	60.48	55.88	62.63	63.92	31.22	1.51	41.49	3.12	9.67	12.13
Chlorite	0	0	0	0	0	0	0	0	0	0.53	0	0	0
RMSE	0.0103	0.0097	0.0098	0.0112	0.012	0.011	0.0148	0.0149	0.018	0.0091	0.012	0.0138	0.0159

Appendix L: Results using the Modified Hand-Picked Library for deconvolution. Figure L1 shows the unmixing results for all samples measured. Figures L2-L4 show the plots for the models created by deconvolution, the measured spectrum, and the residual between the two.

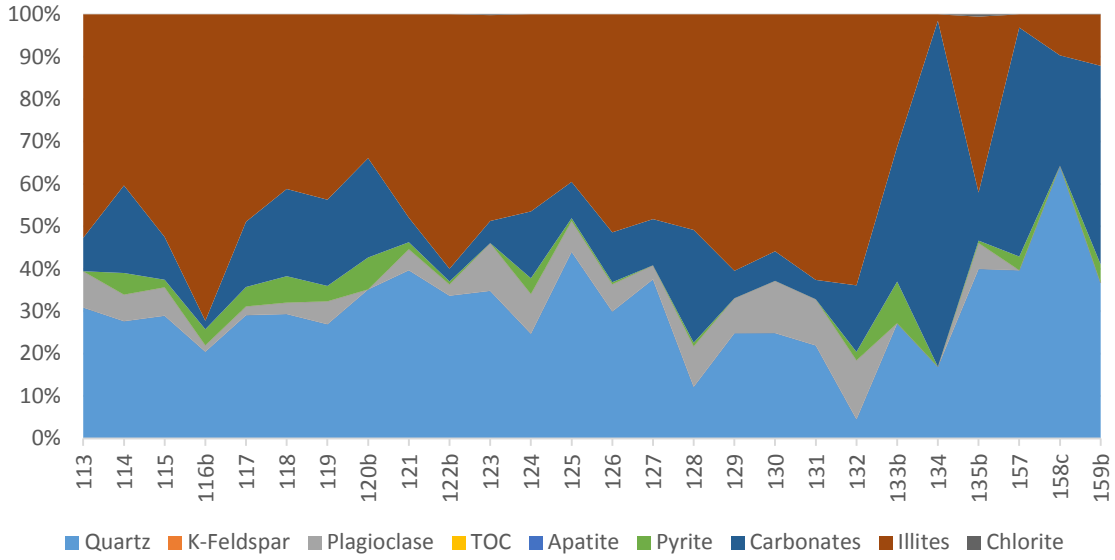

Figure L1: Charted results from using the Modified Hand-Picked Library for deconvolution.

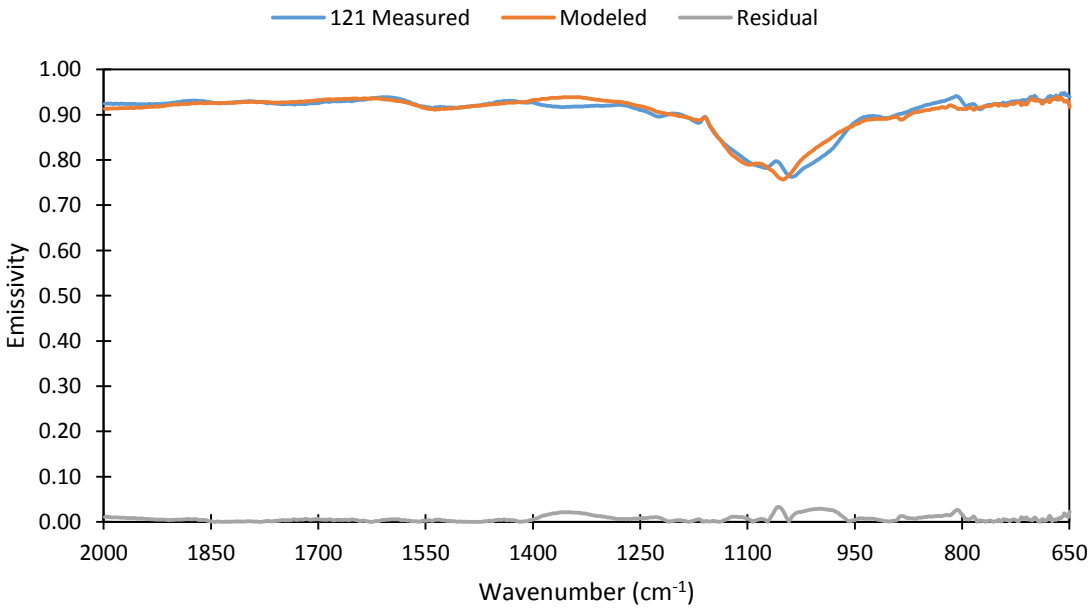

Figure L2: Sample 121 measured and modeled spectra using the Modified Hand-Picked Library.

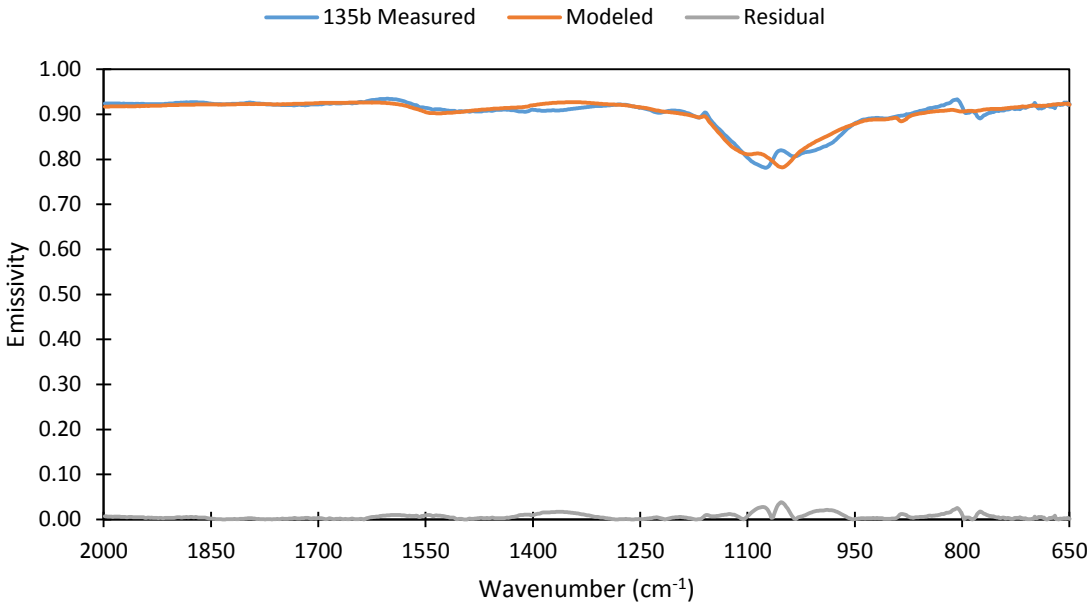

Figure L3: Sample 135b measured and modeled spectra using the Modified Hand-Picked Library.

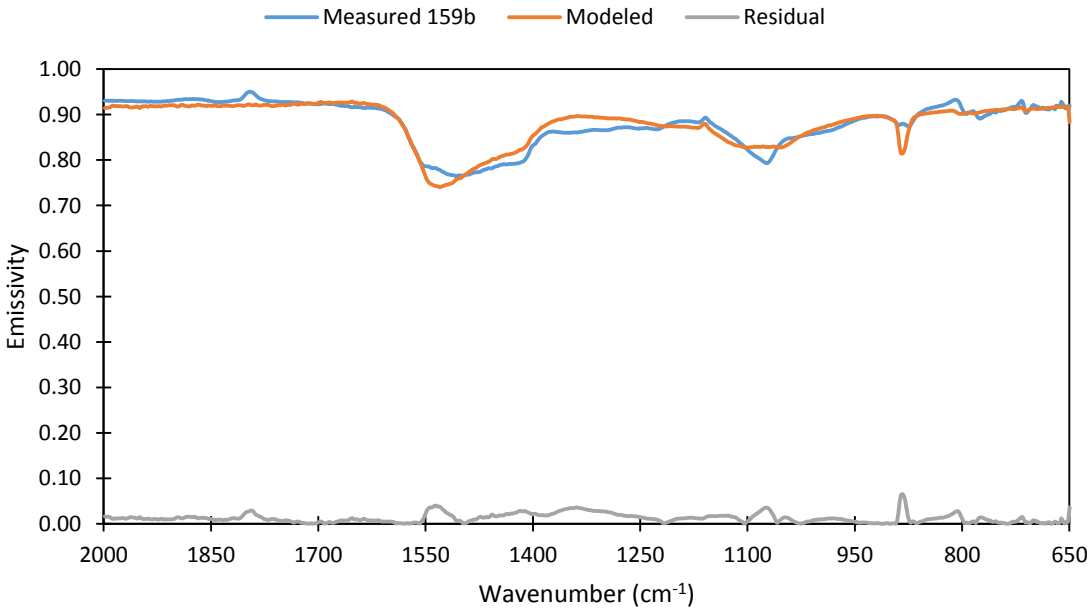

Figure L4: Sample 159b measured and modeled spectra using the Modified Hand-Picked Library.

Appendix M: Tabular side by side comparison of the blind unmixing technique to the XRD data.

Both RMS error rows are conditionally formated showing lower numbers in green, higher numbres in red.

Analysis	FTIR	XRD	FTIR	XRD	FTIR	XRD	FTIR	XRD	FTIR	XRD	FTIR	XRD	FTIR	XRD
Sample ID	113	113	115	115	117	117	119	119	121	121	123	123	125	125
Quartz	0	30.92	0	29.85	0	30.64	0	23.65	6.57	29.62	0	31.40	0	30.50
K-Feldspar	0	0.43	0	0.11	0	0.00	0	0.54	0	0.86	0	0.00	7.34	0.64
Plagioclase	22.6	9.47	21.9	10.47	20.13	9.38	22.4	9.07	6.15	9.49	29.41	9.46	15.37	9.57
TOC	0	4.01	0	4.91	0	3.83	0	3.66	0	3.72	0	3.94	0	3.54
Apatite	0	0.28	0	0.37	0	0.18	0	0.28	0	0.18	0	0.00	0	0.28
Pyrite	0	2.58	18.93	2.20	0	2.42	0	1.87	3.21	2.81	14.92	1.92	5.74	2.47
Carbonates	3.68	4.639334	3.75	6.660065	5.73	6.047085	13.25	20.84329	5.6	5.414503	1.39	8.345177	3.95	4.836997
Illite	66.73	46.75862	55.43	44.60942	69.18	46.29638	55.24	39.35475	63.94	47.07533	51.84	43.7346	67.6	48.17118
Chlorite	6.99	0.92	0	0.83	4.96	1.20	9.12	0.74	14.53	0.83	2.43	1.19	0	0.00
Averaged RMSE	0.012		0.0109		0.0115		0.0178		0.0087		0.0081		0.0094	
RMS from abundance	13.28		12.70		13.39		11.23		10.70		13.68		12.52	

Sample Depth	FTIR	XRD	FTIR	XRD	FTIR	XRD	FTIR	XRD	FTIR	XRD	FTIR	XRD	FTIR	XRD
Sample ID	127	127	129	129	131	131	133b	133	135b	135	157	157	159b	159
Quartz	0	25.82	2.5	26.34	0	25.83	0	27.93	4.13	39.47	0	17.55	0	26.65
K-Feldspar	0	0.43	0	0.22	12.82	0.54	4.93	0.00	0	0.00	0	0.00	0	0.00
Plagioclase	18.46	9.20	1.05	11.03	0	11.24	25.52	10.28	23.47	11.04	2.45	2.71	0	2.10
TOC	0	4.12	0	4.76	0	5.05	0	7.27	0	7.34	0	0.89	0	4.29
Apatite	0	0.18	0	0.19	0	0.28	4.77	0.38	0	0.37	0	0.18	0	0.00
Pyrite	0	2.37	3.08	3.89	0	4.01	27.54	4.60	19.32	3.79	0	0.60	0	0.32
Carbonates	6.48	16.65002	3.58	2.932497	2.15	1.495693	7.99	13.39946	7.63	8.743825	53.77	68.36354	43.74	56.98299
Illite	72.7	41.21715	67.42	50.64001	67.1	51.55603	29.24	36.14741	40.11	29.23827	43.76	9.710823	56.26	9.6623
Chlorite	2.36	0.00	22.38	0.00	17.94	0.00	0	0.00	5.33	0.00	0	0.00	0	0.00
Averaged RMSE	0.0085		0.0084		0.0085		0.0133		0.0093		0.014		0.0175	
RMS from abundance	14.44		12.80		13.12		13.79		14.32		13.67		18.50	

Appendix N: Tabular side by side comparison of unmixing using the Modified Forward-Mixing library to the XRD data.
Both RMS error rows are conditionally formated showing lower numbers in green, higher numbres in red.

Sample Depth	FTIR	XRD	FTIR	XRD	FTIR	XRD	FTIR	XRD	FTIR	XRD	FTIR	XRD	FTIR	XRD
Sample ID	113	113	115	115	117	117	119	119	121	121	123	123	125	125
Quartz	23.6	30.92	28.75	29.85	29.76	30.64	27.5	23.65	35.04	29.62	32.31	31.40	27.97	30.50
K-Feldspar	0	0.43	0	0.11	0	0.00	0	0.54	0	0.86	0	0.00	0	0.64
Plagioclase	10.21	9.47	8.44	10.47	0	9.38	0	9.07	6.62	9.49	11.72	9.46	9.46	9.57
TOC	0	4.01	0	4.91	0	3.83	0	3.66	0	3.72	0	3.94	0	3.54
Apatite	0	0.28	0	0.37	0	0.18	0	0.28	0	0.18	0	0.00	0	0.28
Pyrite	0	2.58	0	2.20	0.4	2.42	2.61	1.87	0	2.81	0	1.92	0	2.47
Caronbate	5.08	4.639334	7.77	6.660065	11.65	6.047085	20.35	20.84329	4.47	5.414503	4.21	8.345177	4.69	4.836997
Illite	61.12	46.75862	55.05	44.60942	58.19	46.29638	49.54	39.35475	53.87	47.07533	51.76	43.7346	57.88	48.17118
Chlorite	0	0.92	0	0.83	0	1.20	0	0.74	0	0.83	0	1.19	0	0.00
Averaged RMSE	0.0139		0.0123		0.0125		0.021		0.0108		0.01		0.0146	
RMS from abundance	5.62		4.02		5.60		4.90		3.46		3.47		3.65	

Sample Depth	FTIR	XRD	FTIR	XRD	FTIR	XRD	FTIR	XRD	FTIR	XRD	FTIR	XRD	FTIR	XRD
Sample ID	127	127	129	129	131	131	133b	133	135b	135	157	157	159b	159
Quartz	37.44	25.82	24.83	26.34	23.04	25.83	29.19	27.93	34.74	39.47	39.31	17.55	35.07	26.65
K-Feldspar	0	0.43	0	0.22	0	0.54	0	0.00	0	0.00	0	0.00	0	0.00
Plagioclase	0	9.20	8.22	11.03	11.41	11.24	0	10.28	9.52	11.04	0	2.71	0	2.10
TOC	0	4.12	0	4.76	0	5.05	0	7.27	0	7.34	0	0.89	0	4.29
Apatite	0	0.18	0	0.19	0	0.28	0	0.38	0	0.37	0	0.18	0	0.00
Pyrite	0	2.37	0	3.89	0	4.01	2.95	4.60	0	3.79	0	0.60	0	0.32
Caronbate	11.24	16.65002	6.47	2.932497	3.79	1.495693	21.64	13.39946	7.27	8.743825	55.67	68.36354	42.57	56.98299
Illite	51.32	41.21715	60.48	50.64001	61.76	51.55603	46.22	36.14741	48.47	29.23827	5.02	9.710823	22.36	9.6623
Chlorite	0	0.00	0	0.00	0	0.00	0	0.00	0	0.00	0	0.00	0	0.00
Averaged RMSE	0.0099		0.0112		0.0117		0.016		0.0113		0.0127		0.0172	
RMS from abundance	6.44		4.18		4.21		6.08		7.19		8.60		7.17	

Appendix O: Tabular side by side comparison of unmixing using the Modified Hand-Picked library to the XRD data.
Both RMS error rows are conditionally formated showing lower numbers in green, higher numbres in red.

Sample Depth	FTIR	XRD	FTIR	XRD	FTIR	XRD	FTIR	XRD	FTIR	XRD	FTIR	XRD	FTIR	XRD
Sample ID	113	113	115	115	117	117	119	119	121	121	123	123	125	125
Quartz	30.88	30.92	28.93	29.85	29.07	30.64	26.93	23.65	39.67	29.62	34.81	31.40	44.03	30.50
K-Feldspar	0	0.43	0	0.11	0	0.00	0	0.54	0	0.86	0	0.00	0	0.64
Plagioclase	8.52	9.47	6.7	10.47	2.06	9.38	5.4	9.07	4.95	9.49	11.26	9.46	7.26	9.57
TOC	0	4.01	0	4.91	0	3.83	0	3.66	0	3.72	0	3.94	0	3.54
Apatite	0	0.28	0	0.37	0	0.18	0	0.28	0	0.18	0	0.00	0	0.28
Pyrite	0.02	2.58	1.78	2.20	4.57	2.42	3.62	1.87	1.64	2.81	0	1.92	0.63	2.47
Carbonates	7.88	4.639334	10.09	6.660065	15.4	6.047085	20.34	20.84329	5.79	5.414503	5.21	8.345177	8.56	4.836997
Illite	52.71	46.75862	52.5	44.60942	48.91	46.29638	43.71	39.35475	47.95	47.07533	48.56	43.7346	39.51	48.17118
Chlorite	0	0.92	0	0.83	0	1.20	0	0.74	0	0.83	0.18	1.19	0	0.00
Averaged RMSE	0.0124		0.0116		0.0117		0.0208		0.0101		0.0091		0.0109	
RMS from abundance	2.80		3.56		4.36		2.60		3.93		2.75		5.71	

Sample Depth	FTIR	XRD	FTIR	XRD	FTIR	XRD	FTIR	XRD	FTIR	XRD	FTIR	XRD	FTIR	XRD
Sample ID	127	127	129	129	131	131	133b	133	135b	135	157	157	159b	159
Quartz	37.52	25.82	24.83	26.34	21.93	25.83	27.16	27.93	39.98	39.47	39.66	17.55	36.68	26.65
K-Feldspar	0	0.43	0	0.22	0	0.54	0	0.00	0	0.00	0	0.00	0	0.00
Plagioclase	3.3	9.20	8.22	11.03	10.88	11.24	0	10.28	6.09	11.04	0	2.71	0	2.10
TOC	0	4.12	0	4.76	0	5.05	0	7.27	0	7.34	0	0.89	0	4.29
Apatite	0	0.18	0	0.19	0	0.28	0	0.38	0	0.37	0	0.18	0	0.00
Pyrite	0	2.37	0	3.89	0	4.01	9.81	4.60	0.56	3.79	3.23	0.60	4.34	0.32
Carbonates	10.89	16.65002	6.47	2.932497	4.56	1.495693	31.8	13.39946	11.34	8.743825	53.99	68.36354	46.85	56.98299
Illite	48.29	41.21715	60.48	50.64001	62.63	51.55603	31.22	36.14741	41.49	29.23827	3.12	9.710823	12.13	9.6623
Chlorite	0	0.00	0	0.00	0	0.00	0	0.00	0.53	0.00	0	0.00	0	0.00
Averaged RMSE	0.0097		0.0112		0.011		0.0149		0.0091		0.012		0.0159	
RMS from abundance	5.56		4.18		4.59		7.81		5.23		9.15		5.25	

Appendix P: Mineral RMS error relative to XRD measurements. Blue line (XRD) show error bars of five percent for each sample, for each of the three methods (MFM: Modified Forward-Mixed, MHP: Modified Hand-Picked).

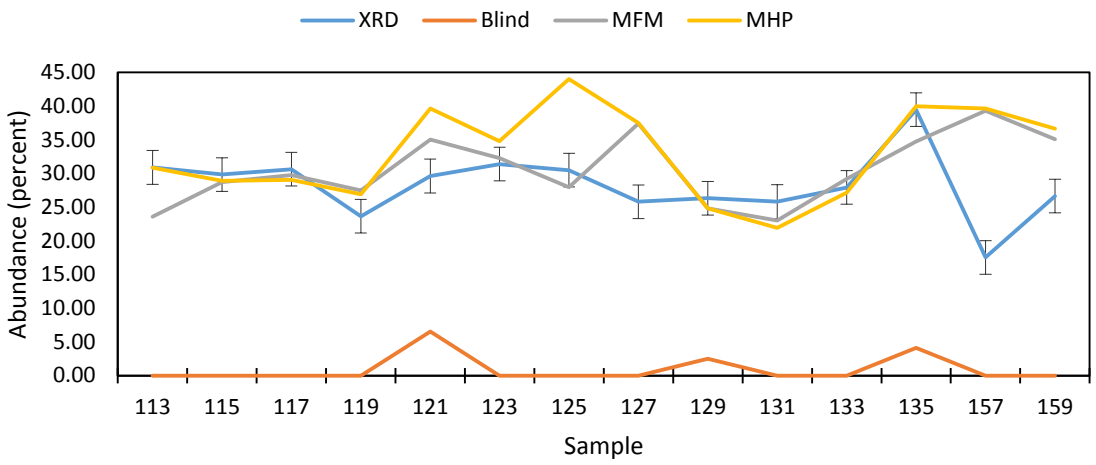

Figure P1: Mineral abundance RMS errors for quartz.

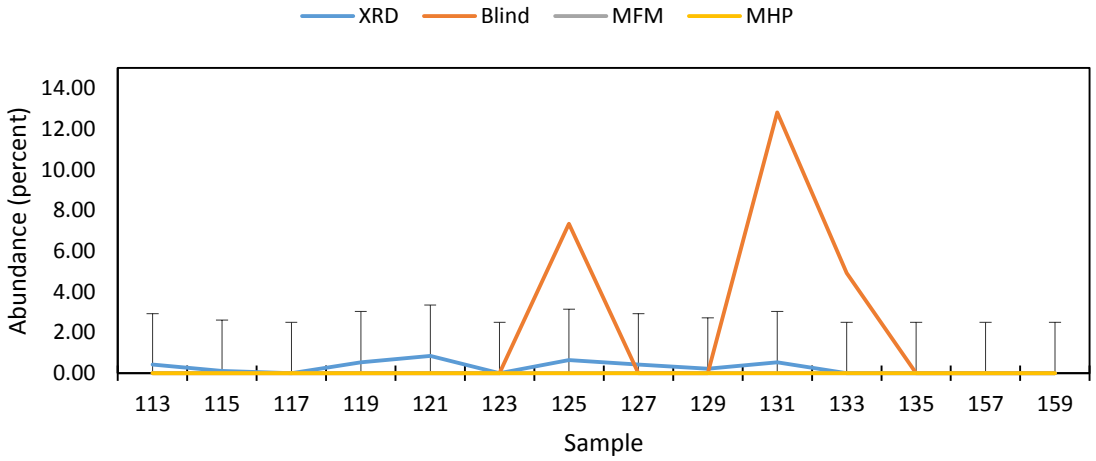

Figure P2: Mineral abundance RMS errors for K-feldspar.

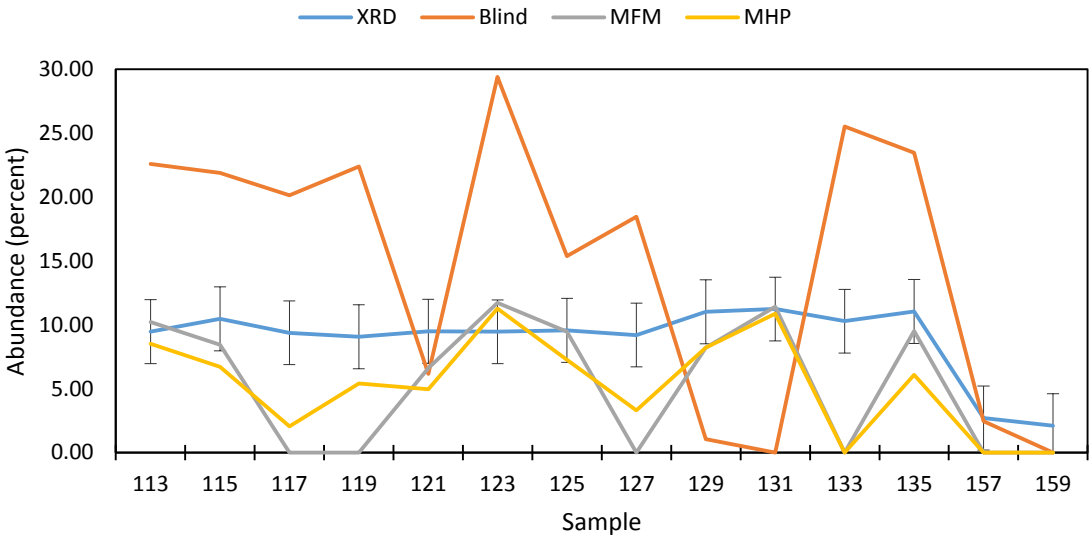

Figure P3: Mineral abundance RMS errors for plagioclase.

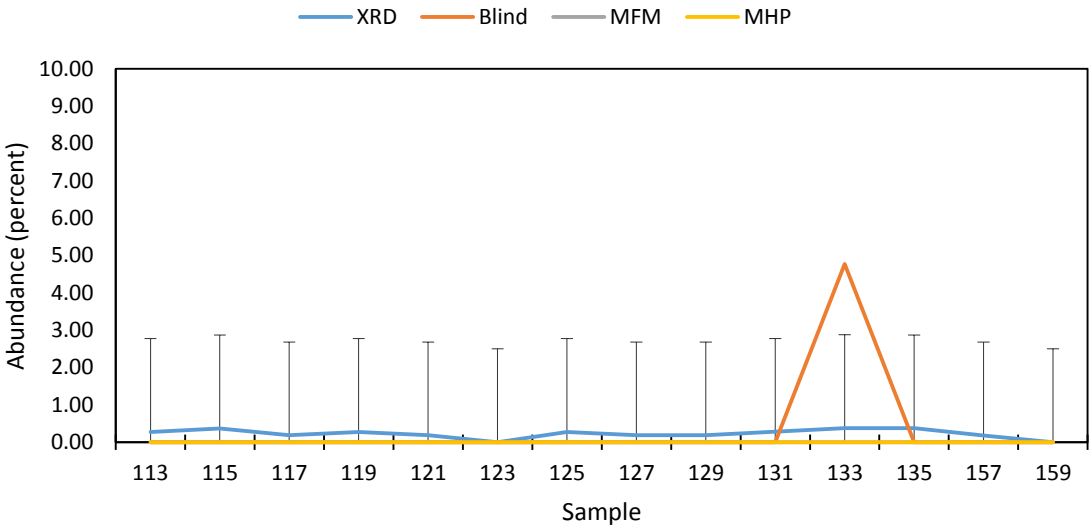

Figure P4: Mineral abundance RMS errors for apatite.

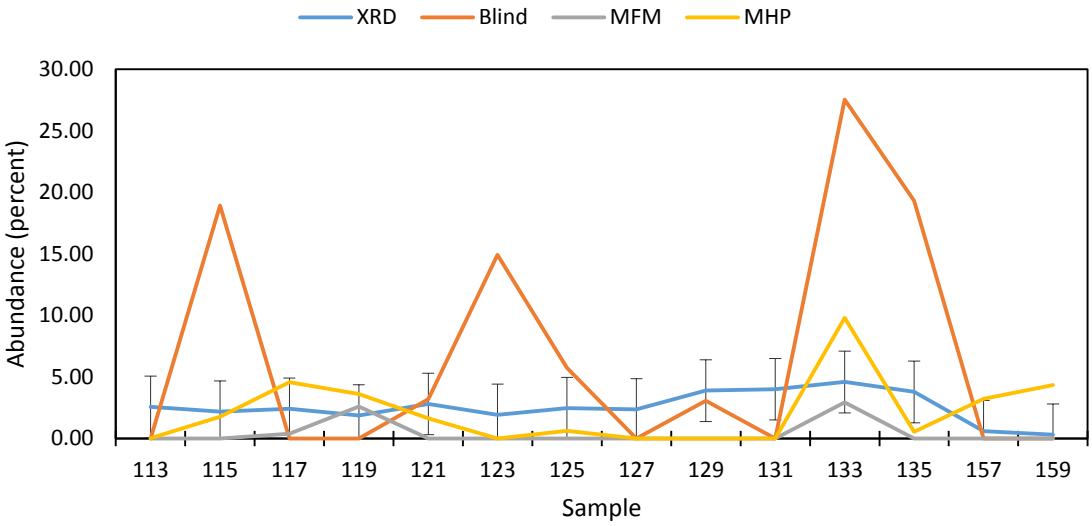

Figure P5: Mineral abundance RMS errors for pyrite.

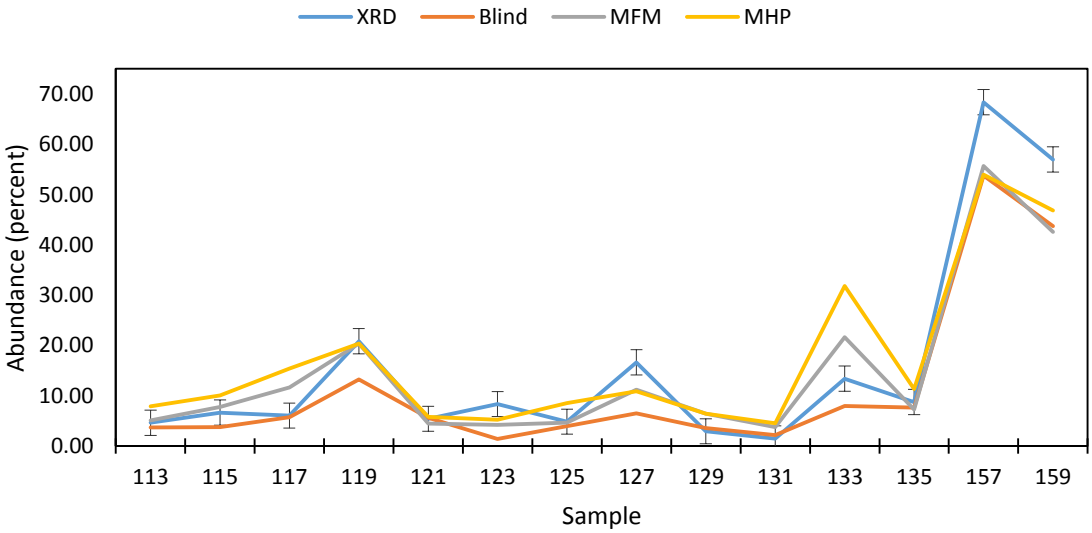

Figure P6: Mineral abundance RMS errors for carbonates.

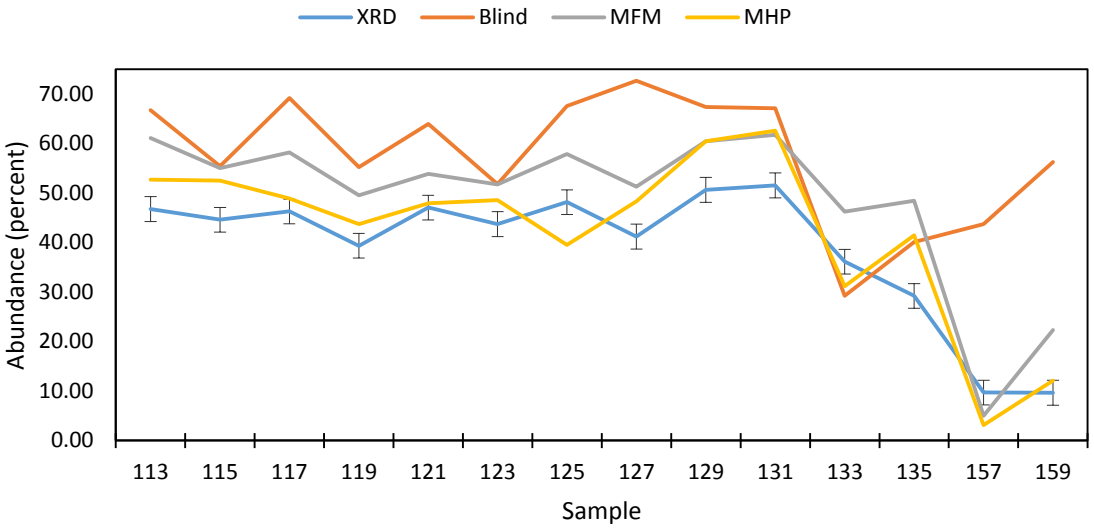

Figure P7: Mineral abundance RMS errors for illite.

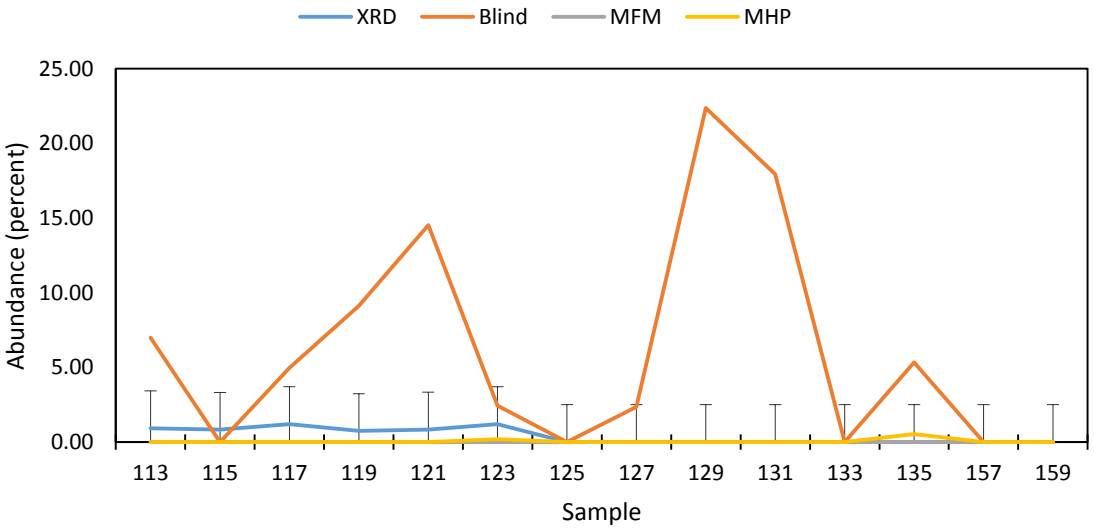

Figure P8: Mineral abundance RMS errors for chlorite.

VITA

Logan Arron Chatterton

Candidate for the Degree of

Master of Science

Thesis: SPECTRAL ANALYSIS OF PETROLEUM RESERVOIR ROCK USING FOURIER TRANSFORM INFRARED (FTIR) SPECTROSCOPY

Major Field: Geology

Biographical:

Education:

Completed the requirements for the Master of Science in Geology at Oklahoma State University, Stillwater, Oklahoma in July, 2015.

Completed the requirements for the Bachelor of Science in Geology at Oklahoma State University, Stillwater, Oklahoma, in 2013.

Experience:

Geologist with Concho Resources, Midland, TX, July 2015

Exploration Geology Intern with Concho Resources, Midland, TX, summer of 2014

Field Geology Intern with Nomac Geo Services, Oklahoma City, OK, summer of 2013

Student Hydrologist with the United States Geological Survey, Oklahoma City, OK, March 2012- May 2013.

Professional Memberships:

President of Geology Graduate Student Association (GGSA) 2013-2014
AAPG